Xu *et al. Energy Mater* 2024;4:400066
DOI: 10.20517/energymater.2023.94

Energy Materials

Review

Open Access

Check for updates

Emerging application of 2D materials for dendrite-free metal batteries

Mengyang Xu[1,#], Zongyuan Xin[1,#], Jun Wang[1], Tsz Wing Tang[1], Yaxuan Li[1], Yuyin Li[1], Tae-Hyung Kim[2], Zhengtang Luo[1,3,*]

[1]Department of Chemical and Biological Engineering, Guangdong-Hong Kong-Macao Joint Laboratory for Intelligent Micro-Nano Optoelectronic Technology, William Mong Institute of Nano Science and Technology and Hong Kong Branch of Chinese National Engineering Research Center for Tissue Restoration and Reconstruction, The Hong Kong University of Science and Technology, Hong Kong 999077, China.
[2]School of Integrative Engineering, Chung-Ang University, Seoul 06974, Republic of Korea.
[3]Hong Kong University of Science and Technology-Shenzhen Research Institute, Shenzhen 518057, Guangdong, China.
[#]Both authors contribute equally to this work.

[*]**Correspondence to:** Prof. Zhengtang Luo, Hong Kong University of Science and Technology-Shenzhen Research Institute, No. 9 Yuexing first RD, Hi-Tech Park, Nanshan, Shenzhen 518057, Guangdong, China. E-mail: keztluo@ust.hk

How to cite this article: Xu M, Xin Z, Wang J, Tang TW, Li Y, Li Y, Kim TH, Luo Z. Emerging application of 2D materials for dendrite-free metal batteries. *Energy Mater* 2024;4:400066. https://dx.doi.org/10.20517/energymater.2023.94

Received: 30 Nov 2023 **First Decision:** 5 Jan 2024 **Revised:** 25 Jan 2024 **Accepted:** 22 Feb 2024 **Available Online:** 8 Apr 2024

Academic Editors: Ho Won Jang, Xiongwei Wu **Copy Editor:** Fanyuan Liu **Production Editor:** Fanyuan Liu

Abstract

Metal batteries using lithium, sodium, potassium, zinc, etc., as anodes have garnered tremendous attention in rechargeable batteries because of their highly desirable theoretical energy densities. However, large-scale application of these metal batteries is impeded by dendrite growth on the anode surface, which may penetrate the separator, leading to battery failure. Two dimensional (2D) materials featured by excellent mechanical strength and flexibility, tunable electronic properties and controllable assembly are promising materials for the construction of dendrite-free metal batteries. In this review, we summarize recent advancements of 2D materials for their potential use in critical components of dendrite-free batteries used as: (1) a host or artificial solid-electrolyte for metal anodes; (2) a solid electrolyte or modifier for electrolyte; and (3) an enhancement component for separators design. We conclude that 2D materials hold great promise for tackling the problems associated with dendrite formation by functioning as mechanical reinforcement and metal deposition regulators, along with improved safety, performance, and durability of batteries. Finally, this review discusses new perspectives and future directions in the field of 2D materials towards safe, high-energy metal batteries.

Keywords: 2D materials, dendrite, metal battery

INTRODUCTION

The growing consumption of fossil fuels and the resulting environmental issues over the last decade have created a pressing need for green energy technologies. Rechargeable lithium (Li)-ion batteries (LIBs) are recognized as a significant replacement for fossil fuels due to their exceptional electrochemical performance and high energy density. The demand for LIBs is expected to rise even further with the proliferation of electronic devices such as smartphones, laptops, and electric vehicles[1-6]. Nevertheless, the energy density of current commercial LIBs is close to its theoretical limit, making it difficult to further increase the battery capacity[7,8]. The increasing price of Li precursors also hinders the sustainable application of LIBs. Although Li-ion batteries had achieved huge commercial success, it is imperative to explore new energy conversion and storage systems that can offer higher capacities and energy densities than current LIBs[9-11].

Due to their low electrochemical potential, excellent theoretical specific capacity and attractive electronic conductivity, metal anodes including Li[12,13], sodium (Na)[14-16], potassium (K)[17,18], zinc (Zn)[19,20], magnesium (Mg)[21], iron (Fe)[22], and aluminum (Al)[23-25] are considered as prospective contenders for next generation rechargeable batteries. Table 1 summarizes the fundamental information regarding various metal anodes[26]. Meanwhile, metal anodes can be paired with various cathode materials, such as sulfur, oxygen, or transition metal oxides, which allows for a wide range of battery chemistry to be developed[27-30]. Additionally, many metals, such as zinc and iron, are abundant and inexpensive, which makes them attractive for large-scale energy storage applications[31-33].

The operational mechanism of metal anodes is similar to that of intercalation-based anodes, with the key difference that metal is directly used as the anode. In this case, instead of the extraction and insertion of ions in the anode, a stripping and deposition process takes place[34]. Meanwhile, a solid electrolyte interphase (SEI) is formed on the metal anode surface due to the reaction between liquid electrolyte components and electrochemically active metal[35]. The SEI layer consists of both inorganic and organic species with high ionic conductivity but is electronically insulating. Another important function of the SEI layer is to inhibit further side reactions between the electrolyte and metal anode. However, challenges related to highly reactive metallic anodes greatly obstruct the practical application of the metal anode-based secondary batteries, which are summarized as follows: (1) metal anodes experience volume changes during cycling, which can cause mechanical stress and fracture of the anode material; (2) Metal anodes are prone to passivation in the electrolyte with inorganic salts/organic solvent owing to the formation of a non-conductive layer on the surface of the anode that reduces its electrochemical activity. The continuous consumption of electrolytes during charging/discharging processes leads to a lower Coulombic efficiency (CE) along with large capacity reduction, resulting in a short lifespan; and (3) The formation of dendrites during cycling. Dendrites are sharp projections that form on the surface of the anode and can penetrate the separator, leading to short circuits and potentially causing safety concerns. In addition, it is possible for the dendrites to detach from the anode surface and generate "dead" metal that floats in the electrolyte. This "dead" metal cannot participate in subsequent cycles, leading to a reduced CE and shorter lifespan. The dendrites will also give rise to an unstable SEI layer. Consequently, the cracks and reconstruction of the unstable SEI layer will accelerate electrolyte decomposition and "dead" metal generation[36-41].

Numerous research has been conducted in the past few decades to determine the mechanism regarding nucleation and growth of dendrites. The lithium dendrites growing over time can be modeled using Sand's time, as proposed by Rosso and Brissot in equation (1)[42-44]:

$$\tau = \pi D\left(\frac{eC_0}{2J}\right)^2\left(1+\frac{\mu_{Li+}}{\mu_a}\right)^2 \quad (1)$$

Where τ denotes the time when dendrites begin to grow, D is diffusion constants, *e* is electronic charge of value, C_0 is initial concentration, *J* represents the effective current density, and μ_{Li+} and μ_a refer to the lithium ionic mobility and anionic mobility. Consequently, the dendrites will generate along with low ionic mobility and high current density, reducing the cyclic lifespan of the metal batteries. Once the concentration of ions on the surface of the metal anode reaches zero, cations and anions in the electrolyte behave reversely, leading to accumulated ions on the anode surface[45-47]. Based on this perspective, the growth and nucleation of dendrites depend on the effective current density distribution and interfacial elastic modulus. A high interfacial elastic modulus is desirable in protective coatings because it enhances the mechanical stability and integrity of the coating. It allows the coating to withstand the stresses and strains that occur during the charging and discharging processes of the battery[35].

Since the discovery of graphene in 2004, the energy community has extensively researched two dimensional (2D) materials to tackle the current obstacles associated with electrodes and electrolytes in rechargeable batteries. With the advancement of 2D material manufacturing processes, numerous advanced manufacturing technologies, such as Chemical Vapor Deposition (CVD), Molecular Beam Epitaxy (MBE), Pulsed Laser Deposition (PLD), Scalable Exfoliation (SE), etc., have been extensively researched and developed[48-50], leading to more feasible large-scale, low-cost production of 2D materials. Recently, 2D materials have been considered as a promising solution for addressing the challenge of dendrite formation in metal anodes[51-53]. With their large surface area, 2D materials can provide a large number of nucleation sites for metal deposition and reduce the likelihood of dendrite formation[54]. Additionally, some 2D materials have been found to have catalytic activity for metal nucleation and deposition, which can further enhance the uniformity and stability of metal deposition on the anode surface[55]. Moreover, the mechanical flexibility and chemical stability of 2D materials enable accommodation of the volume changes during cycling, reducing the mechanical stress and fracture of the anode material. Therefore, the development of 2D materials for dendrite-free metal batteries holds great potential toward the development of safe, cost-efficient, and high-energy-density batteries.

In this review, we focus on the application of 2D materials for dendrite-free metal batteries. Firstly, we present a comprehensive scope of the development of 2D materials classification and synthesis methods. Next, we explored the distinctive attributes and functions of these materials and their ability to modify various vital parts for dendrite-free batteries, such as anodes, electrolytes, and separators, as shown in Figure 1. Lastly, we offer insights into the progress of next-generation high-performance dendrite-free metal batteries.

PROPERTIES AND SYNTHESIS OF 2D MATERIALS

Commonly, 2D materials display robust in-plane interaction but weak van der Waals force between their layers. Typically, they are only a few atoms thick in the plane but can extend over a significant area in the other dimensions. These materials often demonstrate exceptional properties that are not present in their bulk forms, including high surface-to-volume ratios, customizable electronic and optical characteristics, and mechanical flexibility. Herein, the properties and synthesis of various 2D nanomaterials, including graphene, transition metal disulfides (TMDs), hexagonal boron nitride (hBN), 2D metal-organic frameworks (MOFs), 2D covalent organic frameworks (COFs), MXene, layered metal (hydro)oxides, and

Table 1. Comparison of various metal anodes

Metal	Li	Na	K	Zn	Mg	Fe	Al
Active ion	Li^+	Na^+	K^+	Zn^{2+}	Mg^{2+}	Fe^{2+}	Al^{3+}
Ionic radius (Å)	0.76	1.02	1.38	0.75	0.72	0.78	0.53
Density (g cm^{-3})	0.53	0.97	0.86	7.13	1.74	7.87	2.70
Potential *vs.* SHE (V)	-3.04	-2.71	-2.93	-0.76	-2.36	-0.45	-1.68
Earth abundance (ppm)	18	23000	21000	79	23000	46500	82000
Melting point (°C)	180	98	63	419	651	1538	660
Specific volumetric capacity (mAh cm^{-3})	2061	1129	610	5855	3834	7558	8046
Specific gravimetric capacity (mAh g^{-1})	3860	1166	687	820	2206	960	2980

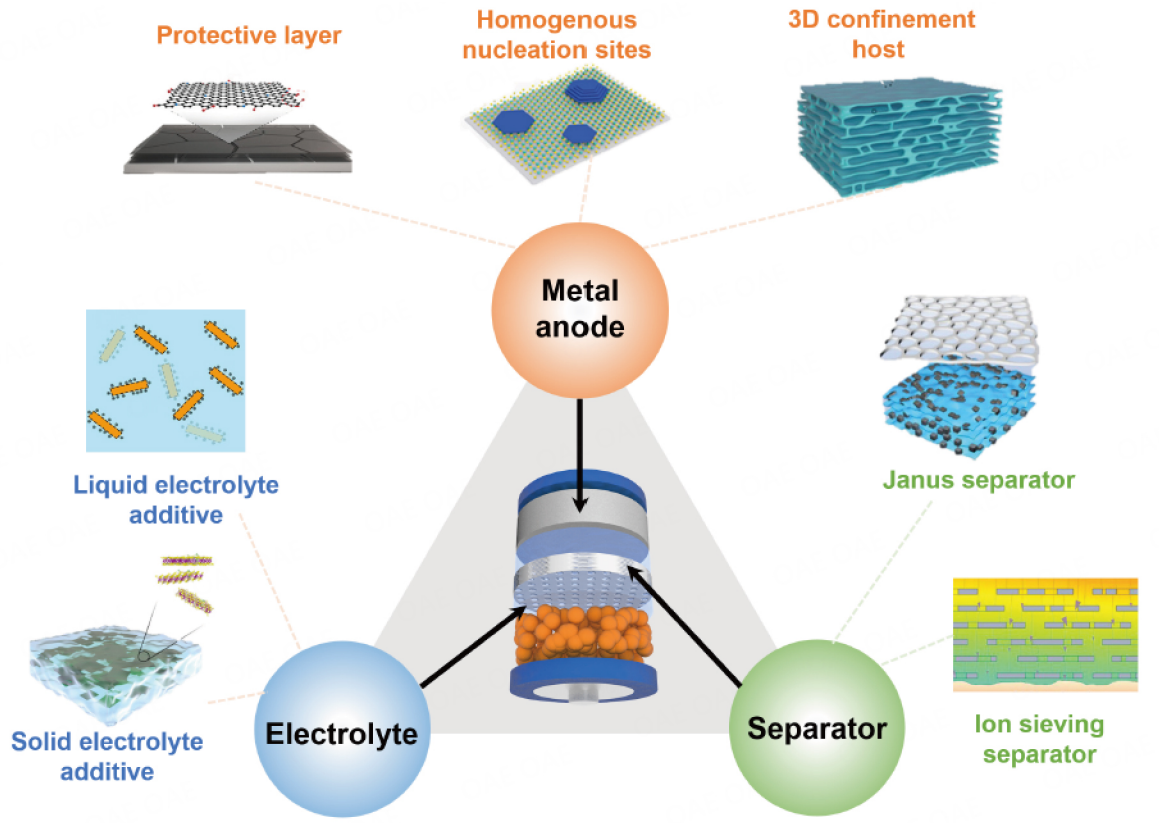

Figure 1. Overall schematic diagram of 2D materials applications toward metal anode, electrolyte, and separator design for dendrite-free metal batteries.

phosphorene, are presented in detail. The production methods of 2D materials are mainly divided into "top-down" exfoliation and "bottom-up" synthetic approaches, as shown in Figure 2. The choice between "top-down" exfoliation and "bottom-up" synthetic approaches depends on factors such as the desired 2D material, scalability requirements, and specific application needs. While "top-down" methods allow for the isolation of high-quality 2D materials from bulk sources, "bottom-up" approaches provide controlled synthesis and assembly of 2D materials with tailored properties. Researchers continue to explore and refine these techniques to enhance the production efficiency, scalability, and quality of 2D materials for various applications.

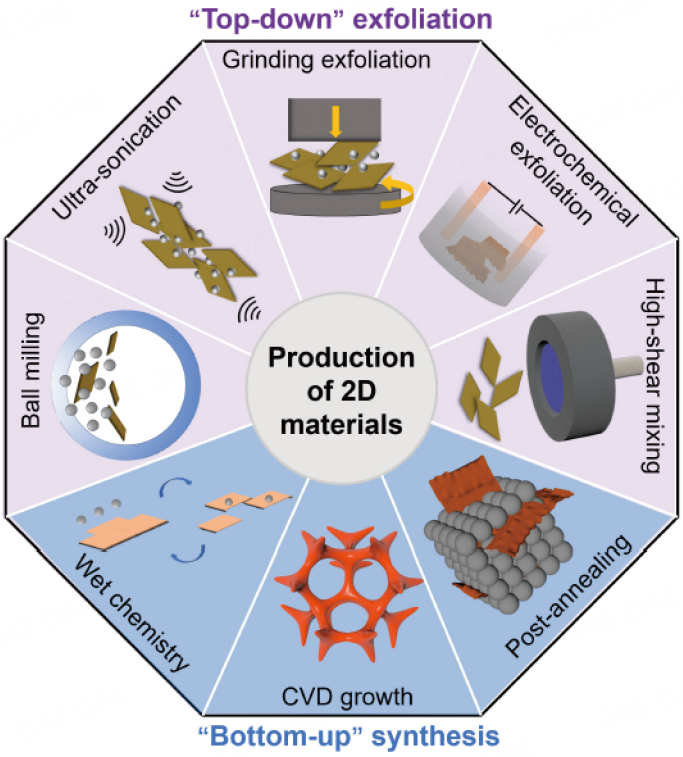

Figure 2. An overview of production methods of 2D materials.

Graphene

Graphene comprises a single layer of graphite, featuring sp^2 hybridized carbon arranged in a hexagonal lattice. It exhibits remarkable mechanical strength (Young's modulus approaches 1 TPa), exceptional thermal conductivity (up to ~5,000 W m^{-1} K^{-1}), and large surface area (2,630 m^2 g^{-1}), while being almost transparent and highly foldable without losing its electrical properties[56-58]. The electronic properties of graphene are particularly noteworthy as they exhibit exceptionally high charge carrier mobilities (exceeding 200,000 cm^2 V^{-1} s^{-1})[59]. This results in ballistic transport, allowing electrons to travel long distances without scattering, making it a fascinating material from a fundamental physics standpoint. The synthesis of graphene can be divided into two main methods: top-down and bottom-up. The top-down approaches isolate graphene from graphite through mechanical or chemical exfoliation, which is known as the "peel-off" method[60]. In comparison, CVD is a widely employed bottom-up method for synthesizing graphene films with controllable thickness, morphology, and tunable mechanical and electronic properties[61]. While large-scale, low-cost production of graphene is still being pursued, high-quality graphene for laboratory use is already commercially available.

Transition metal dichalcogenides

Transition metal dichalcogenides (TMDs), with a general formula of MX_2, are composed of a transition metal (such as Mo, Sn, V, Ti, W, and Ta) and a chalcogen (such as S, Se, and Te). In the typical MX_2 structure, the transition metal M is situated between two chalcogen atoms X, forming an X–M–X layer[62]. TMDs are featured by their versatile crystal structures, ultrathin thickness, tunable band gap, and potential for various functional applications in electronics, optoelectronics, catalysis, energy storage, and other fields[63-65]. Their physical properties are determined by their crystal and electronic structures. For example, the transformation of NbS_2 from 2H to 3R phase results in the disappearance of superconductivity[66], while transitioning the phase of $TaSe_2$ from 2H to 3R significantly increases the superconductivity transition

temperature (from 0.2 to 1.6 K)[67]. Compared to 1H/2H phases, 1T TMDs exhibit metastability and higher electrical conductivity and possess a unique chemical-rich plane[68]. The unique physical, electronic, and chemical properties of TMDs also make them a promising alternative to traditional electrode materials for LIB or sodium-ion battery (SIB) anodes[69,70]. Various synthesis methods are available for producing TMDs, including CVD, mechanical/chemical exfoliation, MBE, hydrothermal methods, salt-templating methods, topochemical transformations, and post-treatment phase transition techniques[71]. High-quality 2D nanosheets, such as $MoTe_2$, TaS_2, and WTe_2, can be obtained through mechanical exfoliation of bulk single crystals of TMDs[72-74]. However, achieving precise control over the size and number of layers in exfoliated flakes poses a challenging task, making it impractical for large-scale commercial applications. Similar to graphene production, CVD methods provide distinct benefits in the production of high-quality, controllable thickness, and large-scale TMDs, establishing an ideal material platform for both theoretical study and practical applications[48,75].

hBN

Despite being an electrical insulator, hBN possesses a remarkably flat surface, high mechanical robustness, and highly stable structure. By employing various methods, it can be altered to achieve different properties and functions. Additionally, 2D-hBN nanosheets possess a hexagonal crystal structure, with lattice parameters of a = 0.250 nm and c = 0.666 nm[76]. These nanosheets are sp^2-hybridized insulators with sublattices arranged in a honeycomb configuration containing equal numbers of B and N atoms. The covalent bonding within each plane results in significant polarization due to the pronounced asymmetry of the sublattices, leading to a wide band gap of 5-6 eV. hBN has potential applications in the field of batteries thanks to its unique traits such as high thermal conductivity, good mechanical properties, and chemical stability. These properties make it an assuring candidate as a heat sink material in LIBs, which generate heat during operation. Additionally, hBN can be used as a protective coating for battery electrodes to enhance their stability and prevent degradation[77]. Top-down strategies to prepare monolayer and few-layer hBN mainly include mechanical and liquid-phase exfoliation from the bulk material[78]. However, the size of as-prepared hBN is limited to a few tens of micrometers with a lack of uniformity and reproducibility. Bottom-up approaches, such as CVD and physical vapor deposition, involve building hBN from its constituent elements to 2D hBN nanosheets. Various metal substrates, such as Ni[79], Cu[80], Fe[81], etc., have been used to catalyze hBN growth. The solubility difference of B and N atoms in substrates determines the size and morphology of hBN. Researchers are also exploring the direct preparation of hBN films on insulating substrates (e.g., silica[82] and c-sapphire[83]) to avoid film damage caused by the transfer process.

MOFs and COFs

MOFs and COFs consist of metal or organic nodes joined by organic linkers to form porous frameworks. The metal nodes can be transition metals, main group elements, or lanthanides, and the organic ligands can be a variety of functional groups such as carboxylic acids, pyridine, or imidazole. Compared to MOFs, COFs do not contain metal ions or clusters, and the organic nodes are linked by strong covalent bonds, resulting in more stable structures. Although their limited electrical conductivity and structural instability under harsh conditions may hinder their effectiveness, their high surface area and tunable pore size offer efficient mass transport and high selectivity, making them a suitable material for catalyzing various chemical reactions in batteries[84]. MOFs and COFs can serve as electrode materials in batteries and can be modified with various functional groups to improve their electrochemical properties, making them a promising material for the development of high-performance and sustainable batteries[85]. In addition, they can be used as protective coatings for battery electrodes to improve their stability and prevent degradation[86]. Several methods exist for preparing MOFs and COFs; for example, certain notable MOFs have been successfully synthesized through direct precipitation at ambient conditions, such as ZIF-8 (Zn(mim)2, mim denotes to 2-methylimidazole), MOF-5, and HKUST-1[87-89]. Hydrothermal and solvothermal synthesis are also

commonly used where soluble precursors self-assemble under high temperatures and pressures[90]. However, significant reaction time and energy input are typically required to achieve thermodynamic equilibrium; therefore, new energy sources have been utilized to facilitate the production of MOFs and COFs. For instance, microwave synthesis offers rapid and efficient synthesis of nanoporous materials with exceptional size distribution and phase selectivity[91]. Mechanochemical synthesis involves grinding or milling together metal ions and organic ligands or nodes in the presence of a solvent or grinding agent, resulting in highly crystalline materials with unique properties[92]. Other alternative methods, such as photochemical[93], electrochemical[94], and electron beam irradiation-assisted synthesis[95], are also widely studied. Despite complex synthesis processes and challenges in large-scale production that pose obstacles to practical implementation, ongoing research aims to address these issues and develop more efficient and stable MOFs and COFs for dendrite inhibition in batteries.

MXene

MXene is an emerging category of 2D material with the formula of $M_{n+1}X_nT_x$, where M represents early transition metals (such as Ti, V, Mo, etc.), X is carbon and/or nitrogen (N), and T stands for the surface functional groups (O, OH, Cl, F, etc.), which may differ depending on different preparation methods[96]. MXene possesses remarkable electrical, mechanical, and chemical properties, which enable its application in broad research fields. Its electronic conductivity is within the range of 6000-8000 S cm^{-1}, which is comparable with that of multilayered graphene and superior to that of carbon nanotubes (CNT) and reduced graphene oxide (rGO)[97]. Through first-principles calculations, Young's modulus of bare Ti_2C, Ti_3C_2, and Ti_4C_3 are predicted to be 597, 502, and 534 GPa, respectively, and the maximum strain that 2D Ti_2C can endure is calculated to be 9.5% biaxially and 18% uniaxially[98]. MXenes synthesized via a wet-chemical etching method always have rich functionalities such as oxygen or halide-containing groups on the surface, which offer abundant chances for termination modification; for example, the -F can be removed by heat treatment in vacuum, which will influence the band structure of MXenes and thus enhance the electrical performance[99]. Reductive atmosphere and alkaline additives will increase the content of O-containing surface functional groups (-O and -OH); thus, the hydrophilicity can be improved[100]. The first MXene $Ti_3C_2T_x$ was synthesized by Naguib *et al.* through room temperature exfoliation of Ti_3AlC_2 in hydrofluoric acid (HF)[101]. It was achieved by selectively etching the A atomic layer (usually Al, Si, Sn, etc.) of the MAX phase, as covalent/ionic M-X bonds are usually stronger than metallic A-A and M-A bonds[102]. Up to now, various MXenes have been synthesized by HF etching because of the simplicity of operation[103], but it poses a significant drawback as it is highly toxic and hazardous. Later, safer etching methods, such as molten salt etching[104], electrochemical etching[105], and alkali etching[106], were developed. Direct synthesis from the bottom up was also reported; for example, Ti_2CCl_2 was successfully fabricated via a CVD method with accurately controlled structures[107]. The CVD approach can not only offer convenience and scalability but also provide new MXenes for mechanism studies and electronic and energy device development.

Layered metal oxides and hydroxides

Layered metal oxides and hydroxides are also a large family of 2D materials, whose formula can be written as M_xO_y and $M_x(OH)_y$, respectively (where M is transition metal atoms such as Ni, Co, Mn, etc.). By virtue of the high surface-to-volume ratio and the fully exposed active sites, layered metal oxides and hydroxides showed considerable electrochemical properties, making themselves promising candidates for electrodes of SIBs or supercapacitors[108]. For example, ultrathin NiO nanosheets prepared by Sun *et al.* showed high stability in specific capacity after 170 cycles at a high current density of 2 A g^{-1}[109]. Besides, the morphologies of layered metal oxides are tunable through control of parameters such as pH values, temperature, annealing time, etc., to acquire samples with different electrochemical performance[110]. Normally, layered metal oxides are prepared from corresponding layered metal hydroxides through annealing in air, in which a topochemical conversion process happens via dehydration and oxidation[111]. The synthesis of layered

metal hydroxides is quite simple owing to their layered hexagonal crystal nature. The commonly used methods include hydrothermal/solvothermal reactions[112], electrochemical deposition[113], chemical bath deposition[114], etc.

Phosphorene

Phosphorene is composed of sp^3-configured phosphorus atoms that are connected by in-plane covalent bonds and out-of-plane Van der Waals forces. It has a direct band gap depending on layer number (1.73 eV-2.0 eV for single layer, 1.36 eV for bilayer, and 0.3-0.35 eV for 15 layers)[115]. The theoretical carrier mobility of phosphene is calculated to be 10000 $cm^2 \cdot V^{-1} \cdot s^{-1}$ (the experimental value has reached more than 1000 $cm^2 \cdot V^{-1} \cdot s^{-1}$)[116]. The on/off ratio of phosphene-based field effect transistors (FET) can reach 10^4, along with good current saturation and quantum Hall effects[117]. The weak interlayer Van der Waals forces of phosphene make the top-down exfoliation method first applied to prepare 2D phosphene from bulk rhombic black phosphorus crystal. According to different exfoliation ways, it can be further divided into micromechanical exfoliation[118], ultrasonic liquid phase exfoliation[119], and plasma etching methods[120]. Bottom-up methods include CVD and PLD, which can accurately control the structure of phosphorus but need wise selection of the precursors and substrates[121].

2D MATERIALS FOR DENDRITE-FREE BATTERIES

The unique features of 2D materials contribute to their ability to prevent dendrite growth. (1) Excellent mechanical strength: 2D materials possess a distinctive structure, consisting of a single layer of atoms arranged in a flat sheet, which renders them highly suitable for use as protective coatings on the surface of the anode. The dense and impermeable nature of 2D materials can effectively hinder the movement of metal ions and the formation of dendrites. (2) High electrical conductivity: when incorporated into battery electrodes, 2D materials with superior electrical conductivity can facilitate more uniform current distribution across the electrode surface. This uniform current flow helps to mitigate the formation of high-current-density regions, reducing the dendrite growth. (3) Controllable assembly structure: By creating a well-defined and controlled network of ion transport channels, 2D materials can guide metal ions to distribute more evenly across the electrode surface, minimizing the formation of dendrites. (4) High surface area: The introduction of 2D materials can increase the surface energy and modify the surface chemistry of the electrode, leading to reduced nucleation sites for dendrites. With their high surface area, 2D materials can provide a large number of nucleation sites for metal deposition and reduce the dendrite formation[54,55,122]. Thanks to their excellent mechanical strength, high electrical conductivity, controllable assembly structure, and high surface area, 2D materials can be incorporated into battery components to suppress the dendrite growth, as shown in Figure 3. They alter the structures of these components and thus enhance the mechanical, chemical, and electronic properties of the battery with improved safety, performance, and durability.

Anode

2D materials as protective layer

Considering the unique sheet-like ultrathin structure, 2D materials are regarded as promising materials to build artificial protective layer for fabrication of high energy density dendrite-free metal batteries, along with their good mechanical properties, excellent ability for metal ions diffusion, and high stability[55,123]. For example, an ultrathin dual-layer interphase on the lithium metal surface (D-Li) has been recently synthesized via a wet-chemical method[124]. As shown in Figure 4A, this artificial *in situ* formed SEI comprises an organic layer of lithium carboxylate and a thin monolayer of Ti_3C_2 MXene doped with BF_3 (BF_3-MXene). Thanks to the BF_3-MXene outer layer, the lithium metal is shielded from interacting with the electrolyte, resulting in a decreased amount of dead Li and degradation of the electrolyte. The honeycomb-structured lithium carboxylate stabilizes the lithium metal anode and enhances the wetting ability of the

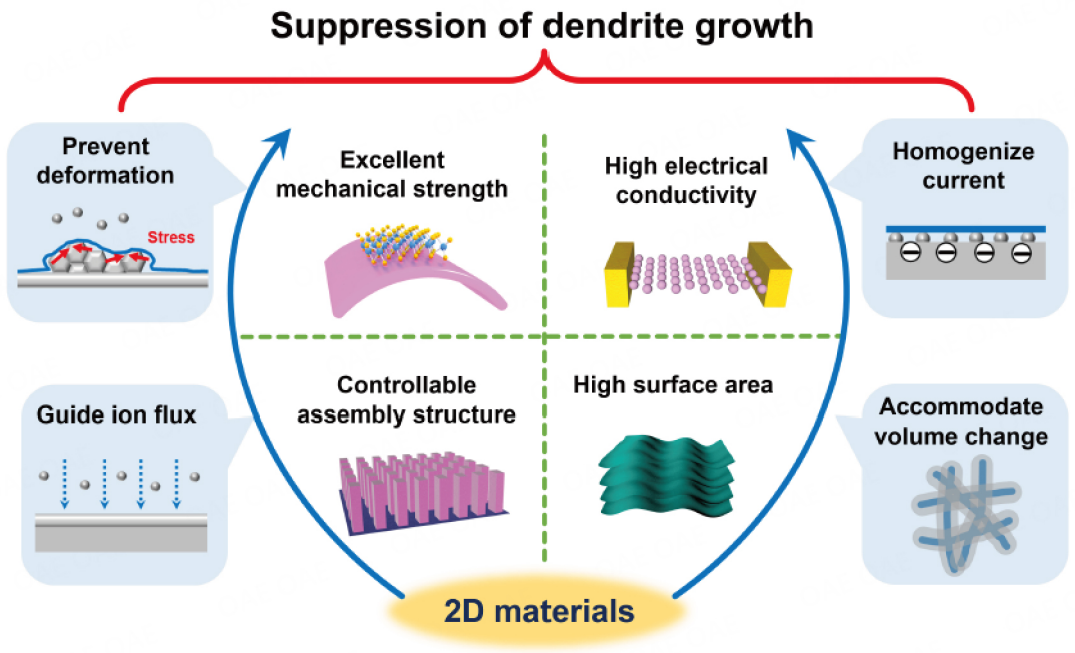

Figure 3. Schematic diagram of the unique features of 2D materials that contribute to their capability in preventing dendrite growth.

interphase towards the electrolyte. As a result, pouch cells with the dual-layer protected lithium anode exhibit excellent stability in 1000 h cycles in symmetric cells with low overpotential, along with superior performance. In addition, Figure 4B highlights a new method for constructing an ultra-thin (less than 1 μm) multilayered protective coating for lithium metal anodes. The coating is composed of nanochannels fabricated by using block-copolymer (BCP), rGO layers, and Ag nanoparticles (Ag NPs)[125]. Synergetic interaction among these three kinds of components in this protective interlayer significantly hinders the uncontrolled lithium dendrite growth. Especially, the highly aligned BCP nanochannels hold a critical role in facilitating the rapid and even distribution of Li-ion transport and providing mechanical reinforcement to the rGO layer. Meanwhile, the Ag NP layer restricts the growth of lithium metal beneath the rGO layer. According to the structural simulations, the multilayered and robust structure can relax the mechanical stress caused by the mossy growth of Li deposition, thereby leading to Li lateral growth and dendrite-free deposition morphology. The full cell pairing of the protected anode and $LiFePO_4$ cathode exhibits exceptional cyclic performance, along with improved rate capability. A similar strategy has also been employed on developing a 2D N-doped graphene oxide (NGO) with an ultra-low thickness of about 120 nm as a protective layer on the zinc metal anode[126]. Figure 4C demonstrates that, in contrast to bare Zn foil surfaces where radical Zn deposition results in dendrite formation and significant side reactions, the NGO protective layer guides the flat deposition of Zn in the (002) planes owing to the parallel graphene layer and the zincophilic properties of the N-doped groups. Consequently, this NGO protective layer results in outstanding energy density in full pouch cell configurations coupled with $LiMn_2O_4$ cathodes. Besides, 2D MOF films can also react as functional interphases towards stable metal anodes[127]. MOF membranes, with adjustable pore structures and pore distribution in the angstrom range, are highly suitable for achieving the separation applications at the ionic/molecular scale[128,129]. For instance, a defect-free artificial SEI based on MOF (ZIF-8) was produced on a magnesium metal anode using an electrochemical deposition technique[130]. This enables selective transport of Mg^{2+} while effectively separating the solvent molecules from the MOF channels, as shown in Figure 4D. The densely packed MOF interlayer effectively mitigates the degradation of the Mg anode by limiting the penetration of solvents, thereby resulting in a remarkable cyclic

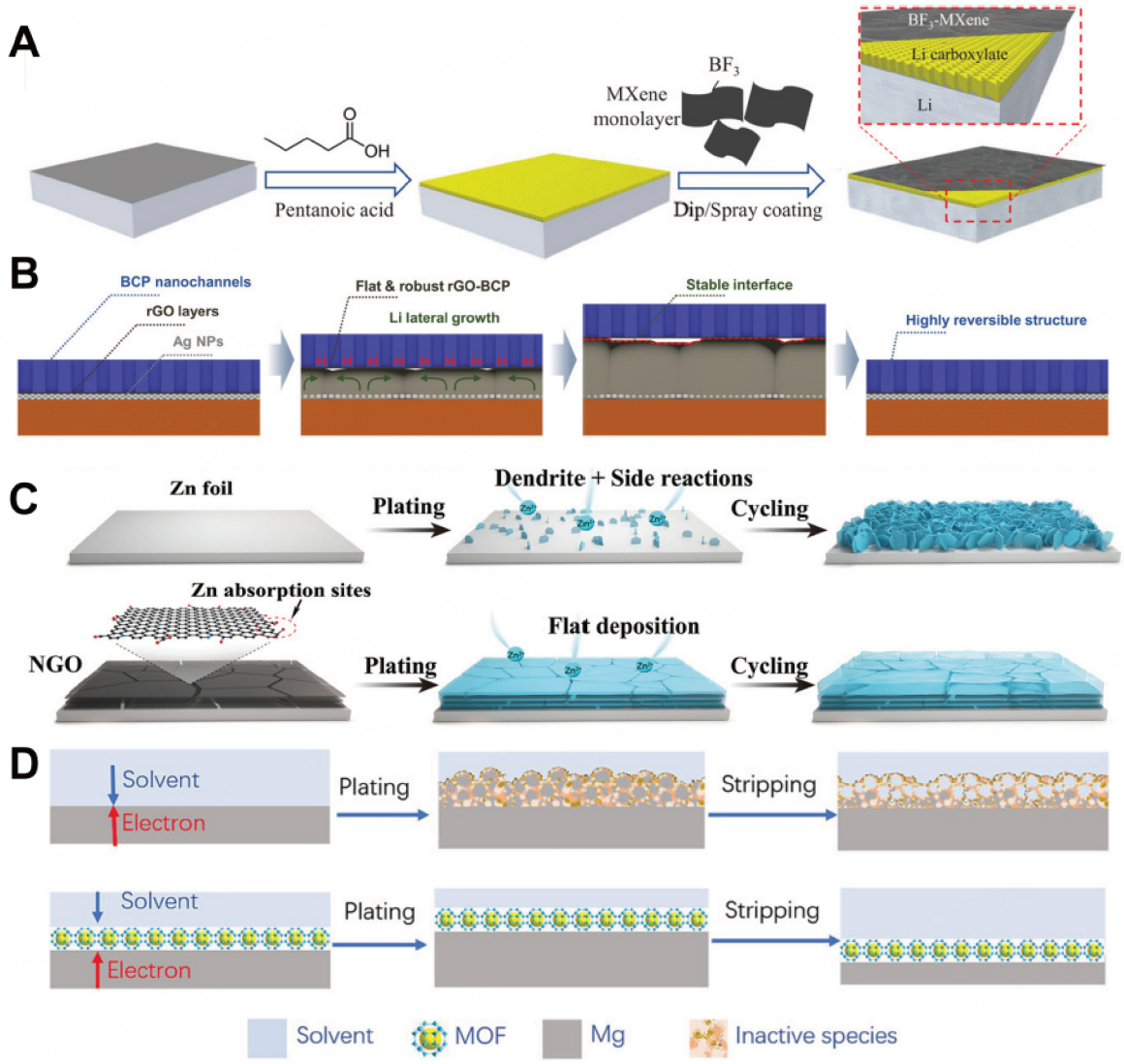

Figure 4. 2D materials as protective layer for metal anodes. (A) Schematic illustration of designed dual-layer coated lithium metal using BF_3-doped Ti_3C_2 MXene. The BF_3-MXene outer layer shields the lithium metal from electrolytes, while Li carboxylates stabilize the lithium metal anode and improve interphase wetting. Reproduced with permission[124]. Copyright 2023, Wiley-VCH GmbH. (B) Graphic visualization of the working principle during lithium plating and stripping process of protectives composed of Ag NPs, rGO layers, and BCP layers on the electrode surface. Reproduced with permission[125]. Copyright 2022, Wiley-VCH GmbH. (C) Schematic illustration of Zn plating on bare Zn foil (upper) and NGO@Zn electrode (lower). The parallelism and zincophilicity of the NGO layer enable the flat deposition of Zn. Reproduced with permission[126]. Copyright 2021, Wiley-VCH GmbH. (D) Suggested degeneration process of bare Mg anode in $Mg(TFSI)_2$/DME, along with the protective impact of a defect-free MOF membrane through precise size-sieve effect of MOF micropores. Reproduced with permission[130]. Copyright 2022, Wiley-VCH GmbH.

stability with low overpotential. Table 2 summarized the recent advancements in 2D materials as protective layer for dendrite-free metal anodes. We conclude that the protective coating composed of different 2D materials on various metal anodes can effectively enhance the cyclic stability and prolong the lifespan.

2D materials as homogenous nucleation sites

Metal ions can be attracted to the 2D material with high surface area due to electrostatic interactions or chemical affinity. Once adsorbed, these ions can undergo nucleation and subsequent growth, forming a uniform metal layer on the 2D material surface. On the one hand, the lattice structure of certain 2D

Table 2. Summary of the reported 2D materials as protective layer for metal anodes

Materials	Electrolyte	Current density (mA cm^{-2})	Capacity (mAh cm^{-2})	Lifetime	Ref.
BF_3-MXene (Li)	1 M LiTFSI in DOL-DME-0.1 M $LiNO_3$	1	1	1000 h	[124]
		5	5	1000 h	
BCP-rGO-Ag NPs (Li)	1 M LiTFSI in DOL-DME-1 wt% $LiNO_3$	1	1	400 h	[125]
$Ti_3C_2T_x$/g-C_3N_4 (Li)	1 M LiTFSI in DOL-DME-1 wt% $LiNO_3$	0.5	0.5	1050 h	[131]
PA-MXene (Li)	1 M $LiPF_6$ in EC-EMC-DMC	1	0.5	900 cycles	[132]
2D MoS_2 (Li)	1 M LiTFSI in DOL-DME	10	10	300 cycles	[133]
$Ti_{0.87}O_2$ nanosheet (Na)	1 M $NaPF_6$ in EC-DEC	1	1	396 cycles	[134]
		5	5	250 cycles	
NGO (Zn)	2 M $ZnSO_4$ aqueous solution	1	1	1200 h	[126]
		5	5	300 h	
MXene/ZnSe (Zn)	2 M $ZnSO_4$ aqueous solution	1	1	2500 h	[135]
		2	1	1500 h	
Defect-free MOF (Mg)	0.5 M $Mg(TFSI)_2$ in DME	0.05	0.05	100 h	[130]

materials can provide a close match with the crystal structure of specific metals. This lattice matching facilitates the nucleation and growth of metal atoms on the 2D material surface. The similar atomic arrangement between the 2D material and the metal promotes the formation of a well-ordered and uniform metal layer. On the other hand, surface defects and edge sites present in 2D materials can act as preferential nucleation sites for metal atoms. These localized regions have different electronic and chemical properties compared to the bulk of electrode hosts, making them energetically favorable for metal nucleation. As a result, 2D materials with high surface area facilitate the uniform deposition of metals reducing the formation of dendrites[136-139].

Based on recent studies, numerous 2D materials such as graphene, N-doped graphene, TMDs, and MXene[51,140-143], are being explored as potential anode substrates for metal deposition on the anode. Our group found that 1T-VSe_2 could be an ideal candidate for Zn regular deposition with a hexagonal shape[144]. As shown in Figure 5A-F, the presence of irregular Zn deposition on a bare Zn surface indicates a random displacement of various grain orientations due to limited Zn mobility and the generation of byproducts. In comparison, highly conductive VSe_2 promotes self-diffusion of Zn adatoms and (002) Zn lattice growth, which results in a shift from random orientation to horizontal stacking. This feature effectively prevents dendrite formation. Archer *et al.*[145] put forward that epitaxial mechanism of Zn deposition on the graphene substrate. Due to the lower lattice mismatch between graphene and Zn, the graphene substrate can ideally regulate the Zn nucleation and distribution as a hexagonal shape. Similarly, Molybdenum disulfide (MoS_2) possesses a layered structure with excellent electrical conductivity, making it suitable for enhancing the performance of battery systems. Alshareef *et al.*[146] successfully fabricated a large-area, mono-oriented MoS_2 substrate in Zn anodes, which effectively guides the non-dendrite Zn deposition and significantly improves the cycling life of Zn-ion batteries [Figure 5G and H]. Wang *et al.*[147] proposed a topological design approach utilizing ultrastrong MXene with abundant lithium nucleation sites, enabling the development of ultrathin and fully flexible lithium metal batteries with improved mechanical strength, cycling stability, and safety. These studies provided compelling evidence of the epitaxial growth mechanism for deposited metal on the substrate, as demonstrated by the meticulous comparison of microstructure changes during plating. The integration of 2D materials as anode substrates holds great promise for achieving enhanced electrochemical performance and stability in metal deposition behavior, paving the path for a more sustainable and efficient future.

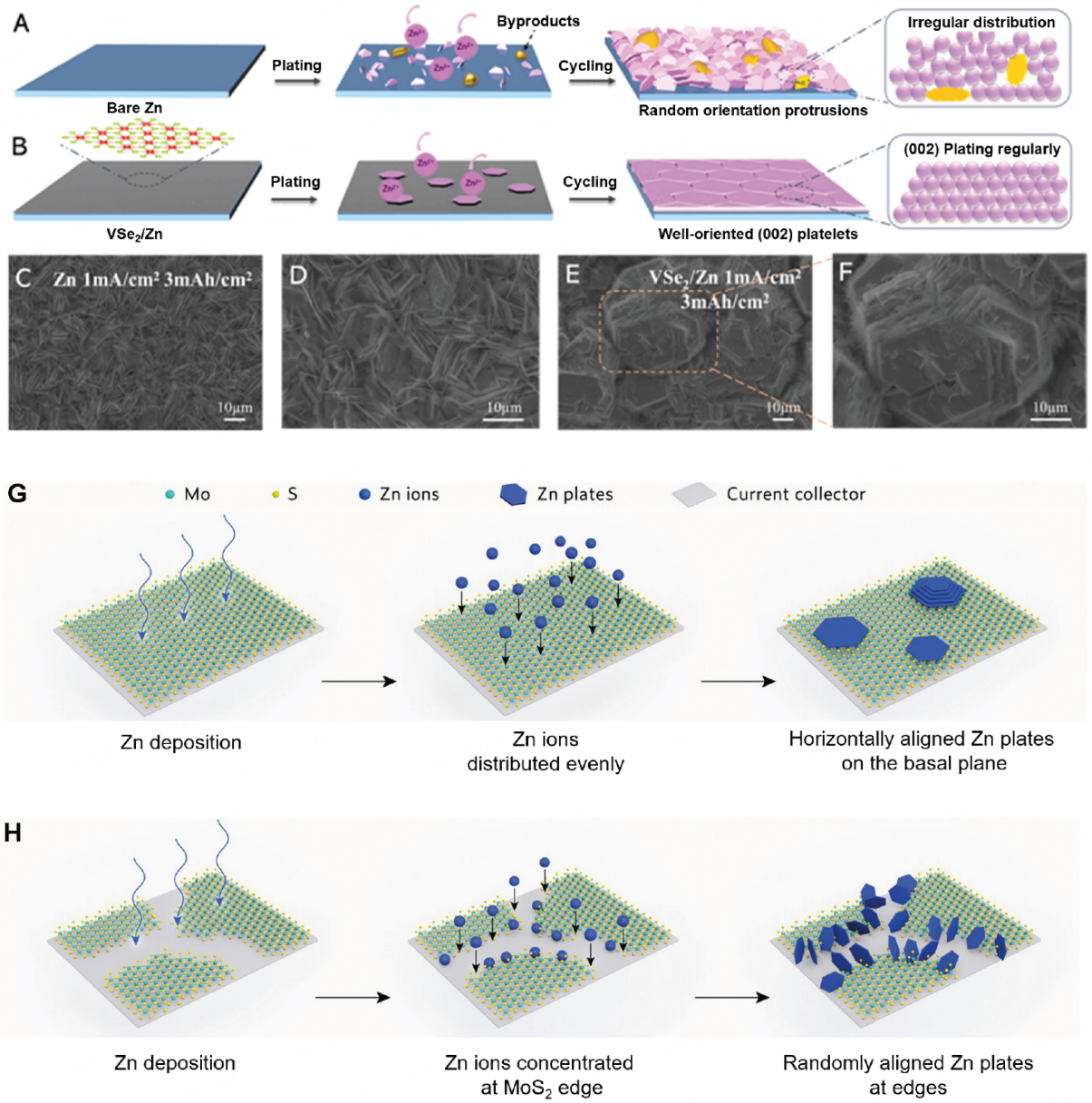

Figure 5. 2D materials as homogenous nucleation sites. (A, B) Deposition mechanism with pure Zn and VSe_2-coated Zn substrate. The rapid diffusion of Zn adatoms on the VSe_2 substrate results in ordered layer-by-layer Zn electrodeposits, which possess a higher portion of the (002) facets. SEM images of deposition morphology on (C, D) bare Zn and (E, F) VSe_2-coated Zn. Reproduced with permission[144]. Copyright 2022, Wiley-VCH GmbH. Potential competitive reaction pathways of Zn deposition on both (G) the basal plane and (H) the edges of a MoS_2 substrate. The basal plane of the mono-oriented MoS_2 substrate effectively guides the non-dendrite Zn deposition. Reproduced with permission[146]. Copyright 2023, Wiley-VCH GmbH.

Controllable assembly of 2D materials as 3D confinement host

Construction of a 3D confinement host presents an effective approach to mitigate the volume change of metal anodes during plating and stripping cycles. Controllable assembly of layered 2D materials can offer ordered porous structure, making it easy for metal to deposit into the interior spaces compared with the traditional 3D substrates such as carbon paper, carbon cloth, porous Cu, etc[148-152]. Furthermore, 3D hosts based on 2D materials with large specific surface area can help alleviate the local current density, homogenize the ion flux, and facilitate uniform metal plating[55]. It is reported that a 3D framework for a

lithium metal anode host was synthesized using a simple ice template-assisted blade coating method[153]. The framework was made by vertically aligned $Ti_3C_2T_x$ MXene nanosheet arrays, as shown in Figure 6A and B. The numerous vertical channels benefit fast Li-ion transportation and uniform Li-ion flux, thus regulating the Li plating behavior and prohibiting the dendrite formation. Therefore, the $Ti_3C_2T_x$ MXene-Li anode exhibits remarkable reversibility and stability in symmetric cells and full cells coupled with $LiFePO_4$ cathodes. Recently, our group also developed a porous graphene foam with SnSe seeds distributed on the surface for stable Na metal anodes via a CVD method[154]. The ultra-light graphene skeleton serves as a free-standing host to offer sufficient space for Na accommodation [Figure 6C] while the SnSe nanoparticles enhance the affinity of graphene for Na. Thermally favorable reaction between metallic Na and SnSe nanoparticles occurs during cycles and generate a dual-nucleation-site interface consisting of $Na_{15}Sn_4$ and Na_2Se. The conversion enables uniform Na nucleation and dendrite-free deposition morphologies on the SnSe@GF electrode, thereby giving rise to excellent stability and low potential hysteresis within 2000 h cycles in the symmetric cells, as displayed in Figure 6D. Also, the fabrication of alkalized Ti_3C_2 (a-Ti_3C_2) nanoribbon architectures as potassium metal anode hosts via alkalization and electrodeposition[155] has been reported. The layer stacked Ti_3AlC_2 MAX is firstly etched by HF to obtain the multilayer Ti_3C_2 (m-Ti_3C_2) MXene. Figure 6E illustrates that the a-Ti_3C_2 electrode with interconnected woven-like structures and abundant potassiophilic sites can effectively facilitate uniform potassium plating and suppress dendrite growth, whereas the delaminated Ti_3C_2 (d-Ti_3C_2) MXene electrode appears the formation of potassium dendrites. Consequently, the a-Ti_3C_2 electrode achieves superior cyclic stability at a high deposition capacity of 10 mA h cm^{-2}. Moreover, advanced technologies such as 3D printing techniques have been employed to controllably assemble the 2D materials for metal anode hosts[156-158]. Wang *et al.*[158] developed a mixture of exfoliated V_2CT_x MXene, graphene oxide (GO) and CNT as ink to obtain the 3D printed V_2CT_x/rGO-CNT aerogel after freeze drying and annealing, as shown in Figure 6F. This artificial microgrid structure with large specific surface area and sodiophilic merit can not only reduce the current density and confine the Na deposition but also promote the electrolyte penetration and homogenize the Na nucleation. Consequently, the as-prepared V_2CT_x/rGO-CNT electrode delivers outstanding stability after more than 3000 h cycles with a high average CE, indicating the promising potential of the advanced 3D printing technique for the advancement of high-performance metal anodes.

Apart from the alkaline metal anodes, 2D materials-based skeleton is also used for the Zn and Al battery system with an aqueous electrolyte. Chen *et al.*[159] developed a MXene/graphene aerogel (MGA) for accommodating Zn through hydrothermal treatment. As shown in Figure 7A, to obtain the MGA free standing host, the mixed hydrogel is dialyzed for 24 hours and placed between two thermal insulation plates and freeze-dried. Then, the composited zinc metal anode is prepared through simple electrodeposition. The zincophilic framework with oxygen functional groups distributes the zinc metal onto the microscale manner, effectively prohibiting the uneven plating and dendrite formation. Figure 7B presents a nanoarray structure made by 2D metal-organic (MOF) flakes, Zn-tetra-(4-carboxyphenyl) porphyrin (Zn-TCPP) for zinc metal anode hosts[160]. As shown in Figure 7C, the simulation result discloses Zn ion distribution on the bare Zn electrode and Zn-TCPP electrode. The Zn-TCPP flakes can guide the current on the electrode after potential is applied, enabling the Zn deposition along flakes. As the Zn-TCPP material is non-conductive, the plating behavior occurs in a bottom-up manner, resulting in a U-shaped deposition and dendrite-free morphology. Yun *et al.*[161] reported a 3D-structured bifunctional MXene paper electrode (3D-BMPE) for aluminum metal battery systems. The porous structure of the 3D-BMPE electrode (as displayed in Figure 7D and E) possesses abundant catalytically active sites for Al redox reactions, thus homogenizing the Al deposition and suppressing the aluminum dendrite formation. The 3D-BMPE with excellent mechanical properties and Al affinity also exhibits significantly improved cyclic stability and rate capability [Figure 7F]. We also summarize the recent advancements in 2D materials as 3D confinement for dendrite-free stable metal anodes, as shown in Table 3.

Table 3. Summary of the reported 2D materials as 3D confinement host for metal anodes

Materials	Electrolyte	Current density (mA cm^{-2})	Capacity (mAh cm^{-2})	Lifetime	Ref.
MXene/ COF (Li)	1 M LiTFSI in DOL-DME-1 wt% $LiNO_3$	1	1	400 h	[162]
Au @ graphene aerogel (Li)	1 M LiTFSI in DOL-DME-0.2 M $LiNO_3$	2	2	1800 h	[163]
		4	4	1200 h	
BC-CNF @rGO (Li)	1 M LiTFSI in DOL-DME-2 wt% $LiNO_3$	2	1	5000 cycles	[164]
		20	1	1000 cycles	
TiNbC-MXene accordion arrays (Li)	1 M $LiPF_6$ in EC-EMC-DEC	5	1	28 000 min	[165]
		20	1	2500 cycles	
SnSe@GF (Na)	1 M $NaCF_3SO_3$ in DEGDME	1	1	2000 h	[154]
		5	5	900 h	
3D-printed rGO/CNT (Na)	1 M $NaPF_6$ in diglyme	2	1	650 h	[156]
		8	1	160 h	
3DP-NGA (Na)	1 M $NaPF_6$ in diglyme	3	1	2000 h	[157]
		5	10	500 h	
3D-printed V_2CT_x/rGO-CNT (Na)	1 M $NaPF_6$ in diglyme	2	10	3000 h	[158]
		5	50	1000 h	
1D/2D $Na_3Ti_5O_{12}$-MXene (Na)	1 M $NaPF_6$ in diglyme	3	3	400 h	[166]
Alkalized Ti_3C_2 (K)	0.8 M KFSI in EC-DEC	5	5	800 h	[155]
		5	10	700 h	
MXene ($Ti_3C_2T_x$)/graphene aerogel (Zn)	2 M $ZnSO_4$ aqueous solution	10	1	1050 h	[159]
MOF flakes (Zn)	2 M $ZnSO_4$ aqueous solution	5	0.5	1880 h	[160]
Zn-MOF-decorated 3D-GC foam (Zn)	1 M $ZnSO_4$ aqueous electrolyte	1	10	2000 cycles	[167]
		1	20	1500 cycles	
MXene (Fe)	0.5 M aqueous $FeSO_4$ solution	0.5	0.5	100 cycles	[168]
3D-structured MXene paper (Al)	$AlCl_3$-[EMIM]Cl	1	1	2000 h	[161]

Electrolyte

2D materials as liquid electrolyte additive

Many efforts have been made to optimize electrolyte composition for suppressing dendrite formation. Electrolyte additives are regarded as a straightforward solution to regulate metal ion deposition. A simple and effective strategy to suppress dendrite formation in lithium metal batteries has been recently reported by utilizing boron nitride nanosheets (BNNSs) as a leveling agent in liquid electrolytes[169]. The boron atoms act as Lewis acid sites that reduce the gradient of Li^+ concentration, enable flattened Li deposition, and adjust to volume changes [Figure 8A and B], leading to over 400h stable cycling [Figure 8C]. Other facile 2D materials, such as tin sulfide nanosheets (TS-Ns), have also been investigated as an additive[170]. As displayed in Figure 8D, highly negatively charged TS-Ns attract significant amounts of Zn^{2+} from the electrolyte and then co-deposit onto the anode, resulting in localized increase in concentration of Zn^{2+} ions. The presence of co-deposited TS-Ns also promotes the homogeneous growth of Zn in the subsequent stages due to their 2D flat structure. With this additive, the Zn||Zn symmetry batteries are capable for more than 1850 stable cycles.

2D materials as solid electrolyte additive

Rational design of solid electrolytes is regarded as an effective method for inhibiting dendrite growth, thanks to their nonflammability and high mechanical modulus. However, solid electrolytes are plagued by

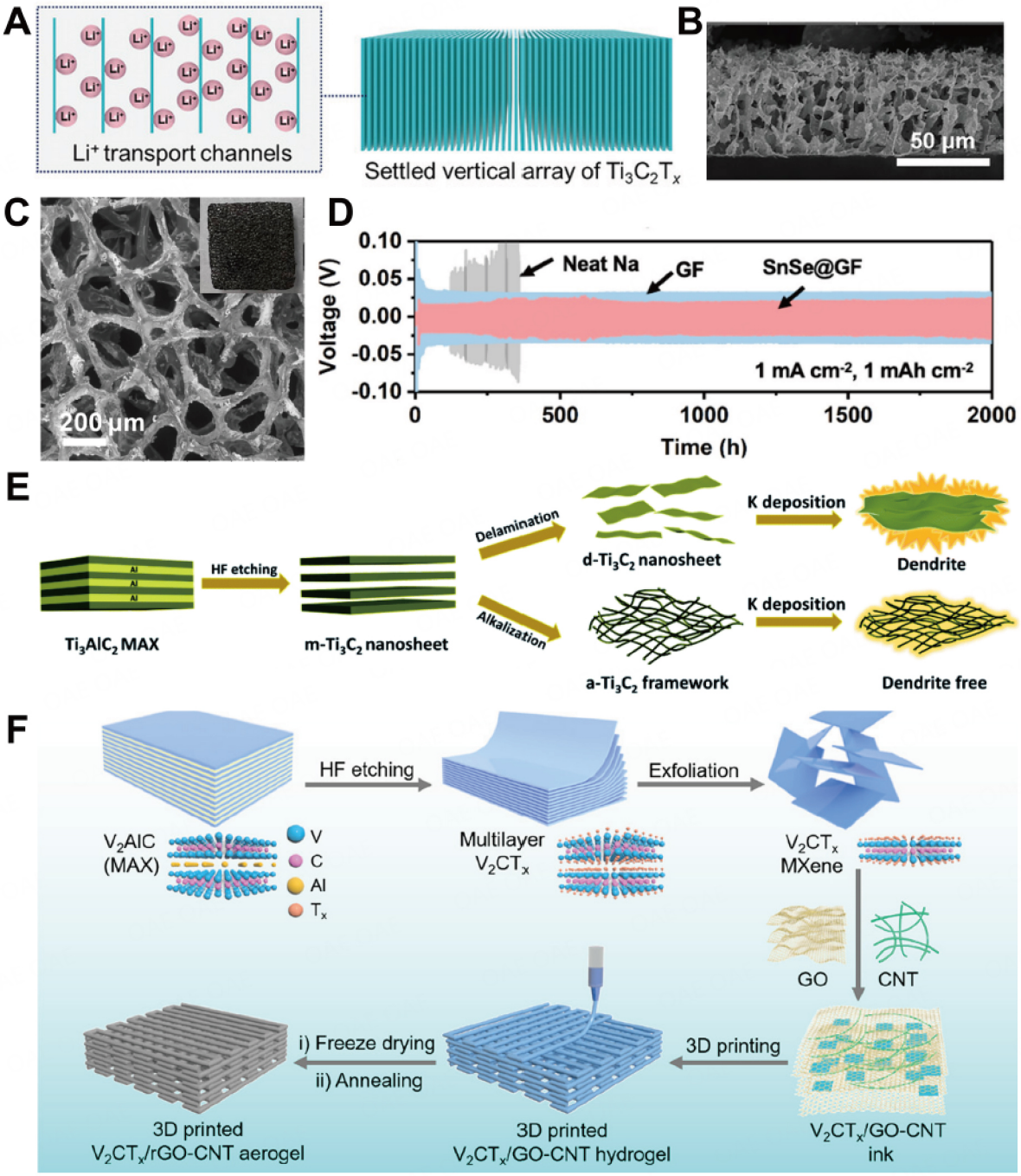

Figure 6. Controllable assembly of 2D materials as 3D confinement host. (A) The graphic visualization of v-$Ti_3C_2T_x$ electrodes. (B) Cross-section SEM image of v-$Ti_3C_2T_x$ electrodes. Reproduced with permission[153]. Copyright 2022, Wiley-VCH GmbH. (C) SEM image of SnSe@GF. (D) Electrochemical charge/discharge voltage curves of the symmetrical cells with pre-sodiated GF and SnSe@GF electrodes measured at an areal current of 1 mA cm^{-2} and a capacity of 1 mAh cm^{-2}, over 2000 hours stable duration was recorded. Reproduced with permission[154]. Copyright 2023, Elsevier. (E) Schematic of the synthesis of a-Ti_3C_2 MXene nanoribbon framework and d-Ti_3C_2 MXene nanosheet for K deposition. Reproduced with permission[155]. Copyright 2020, Royal Society of Chemistry. (F) Schematic diagram of the preparation of a 3D-printed V_2CT_x/rGO-CNT microgrid aerogel electrode through bulk MXene etching and exfoliation, ink synthesis, 3D printing of the hydrogel, and post-treatment. Reproduced with permission[158]. Copyright 2020, Royal Society of Chemistry.

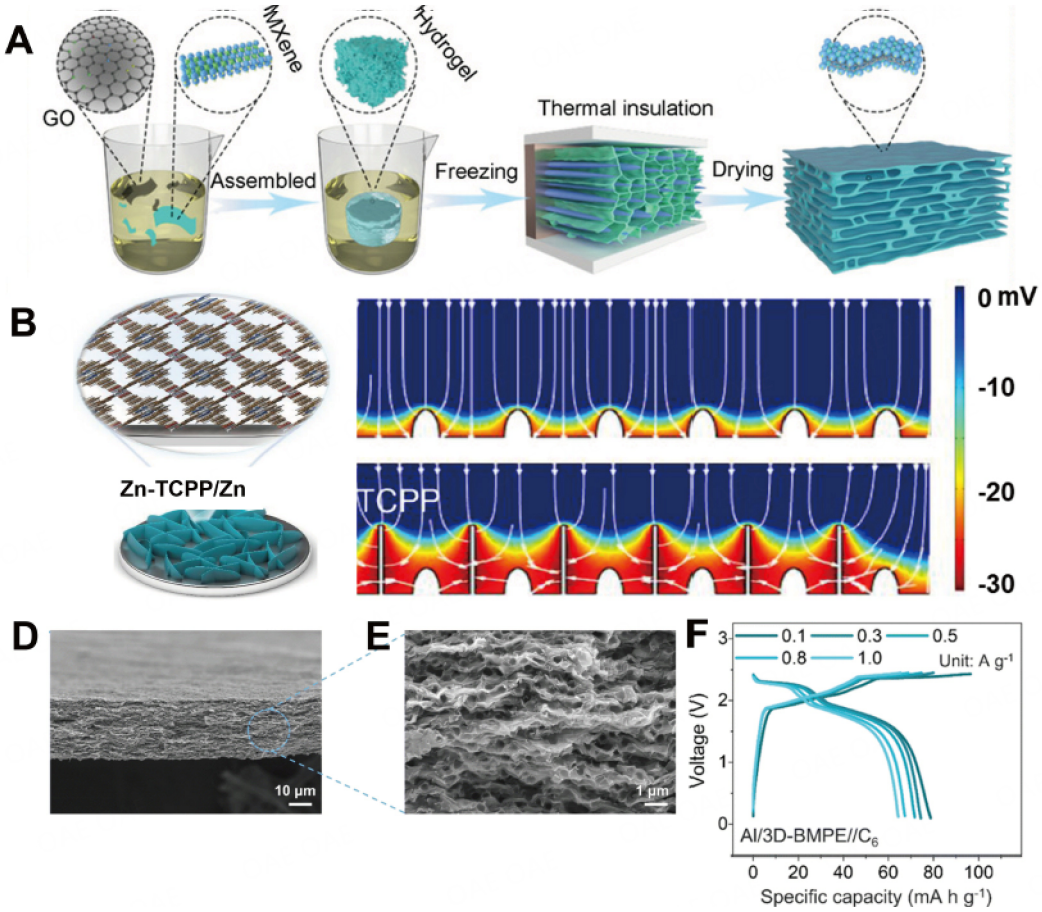

Figure 7. Controllable assembly of 2D materials as 3D confinement host. (A) Schematic illustration of fabricating MGA material. Reproduced with permission[159]. Copyright 2022, Wiley-VCH GmbH. (B) Synthesis scheme of Zn-TCPP/Zn. (C) Simulated potential and current distribution for Zn-TCPP/Zn and bare Zn in a 2 M $ZnSO_4$ electrolyte. The Zn-TCPP flakes guide current on the electrode, facilitating Zn deposition along the flakes, and leading to U-shaped deposition without dendrite formation. Reproduced with permission[160]. Copyright 2022, Elsevier. (D, E) FE-SEM images of 3D-BMPE at different magnifications. (F) Galvanostatic aluminum deposition and dissolution experiments on Al/3D-BMPE//C6 system at various areal current densities. Reproduced with permission[161]. Copyright 2023, Royal Society of Chemistry.

much greater interfacial resistance and poorer ionic conductivity [171], restricting them from broadened applications. Because of their inherent high conductivity and mechanical strength, 2D materials are intensively studied to improve solid electrolytes. For example, a shielding strategy has been applied to enhance the performance of poly(ethylene oxide) (PEO) electrolytes by introducing 2D $Li_{0.46}Mn_{0.77}PS_3$ (LiMPS) nanosheets, which served not only as nano-shields that provided physical protection to the solid electrolytes but also as superior Li^+ absorbers and conductors that regulating Li^+ ion flux [Figure 9A]. Consequently, widened electrochemical window of 4.8V and improved Li conductivity were achieved[172]. The same strategy using 2D-MXene $Ti_3C_2T_x$ was reported to stabilize PEO electrolytes and improve the performance of all-solid-state lithium metal batteries[173]. Liu *et al.*[174] fabricated $Ti_3C_2T_x$-based TiO_2 nanosheets as an additive for gel polymer electrolyte in Zn-ion batteries by a one-stop hydrothermal method, as shown in Figure 9B. Tunable structures and composition of the TiO_2 nanosheets enabled systematic studies about the electrochemical properties under different TiO_2 additions. Benefiting from improved ionic conductivity, higher mechanical strength, and satisfying self-healing ability, over 3000h stable and reversible Zn plating/stripping is achieved.

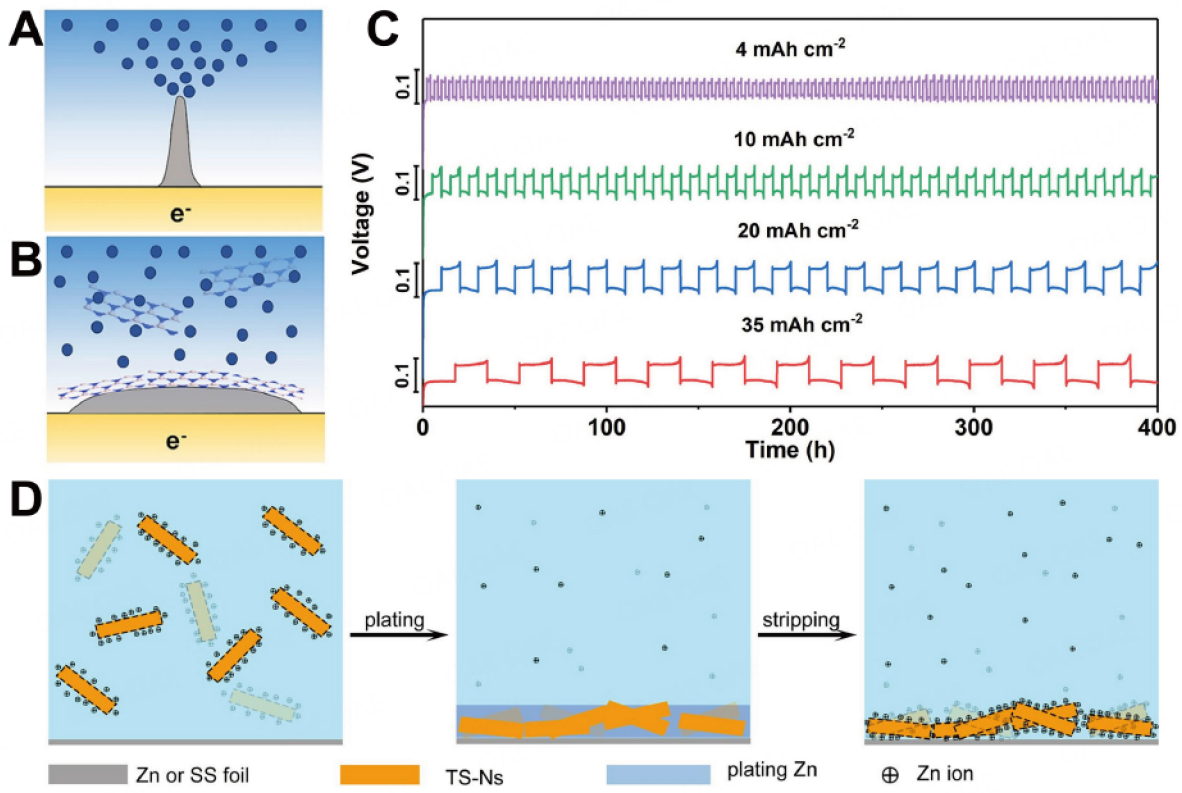

Figure 8. 2D materials as liquid electrolyte additive. (A) A stronger tip electric field leads to the growth of Li dendrites. (B) BNNSs gradually settle at the electrode/electrolyte interface, flattening Li deposition. (C) Voltage-time curves of the Li/Li symmetric cells cycled in the BNNS electrolyte at 2 mA cm^{-2} with over 400h stable cycling. Reproduced with permission[169]. Copyright 2020, Elsevier. (D) Proposed working principle of TS-Ns participated in the Zn plating/stripping. The highly negatively charged ultrathin nanosheets are able to adsorb and then co-deposit the positive zinc ions, which serve as interfacial protection layers around the anode. Reproduced with permission[170]. Copyright 2022, Elsevier.

Separator

2D materials as Janus separator

Aside from electrolytes, the separator is the only other component that comes into direct contact with the anode; hence, modifying the separator is a useful approach to vary metal plating/stripping behaviors and redirecting dendrite growth direction. The rational design of the separator aims to achieve an isotropic distribution of metal ions on the anode surface which facilitates homogeneous nucleation and deposition of metal ions, thus resulting in dendrite suppression.

Conventionally, separators act as electron-insulating and chemically inert components for preventing the direct contact of electrodes, but recent studies have transformed their role from passive to active. The Janus separator, named after the Roman god, with the corresponding functional group coated on each side, has received much attention. For instance, Han *et al.*[175] modified conventional polypropylene (PP) separators by 2D layered MXene (Ti_3C_2X, X= F and O) and solid-state electrolytes ($Li_{1.3}Al_{0.3}Ge_{1.7}(PO_4)_3$, LAGP) in pursuance of planar Li growth on metal anodes, as shown in Figure 10A and B. The improved conductivity facilitates the homogeneous transfer of the Li ions and electrons, and the oxygen and fluorine groups from MXene not only offer more reactive sites and decrease the nucleation energy, but also induce Li atom rearrangement inherited from MXene crystal structures, leading to accumulated capacity of 1000 mAh cm^{-2} and 200 stable cycling performance. Other 2D materials, such as graphitic carbon nitride (g-C_3N_4), have also shown promising potential for dendrite suppression. A 2D g-C_3N_4 nanosheet has been employed to modify

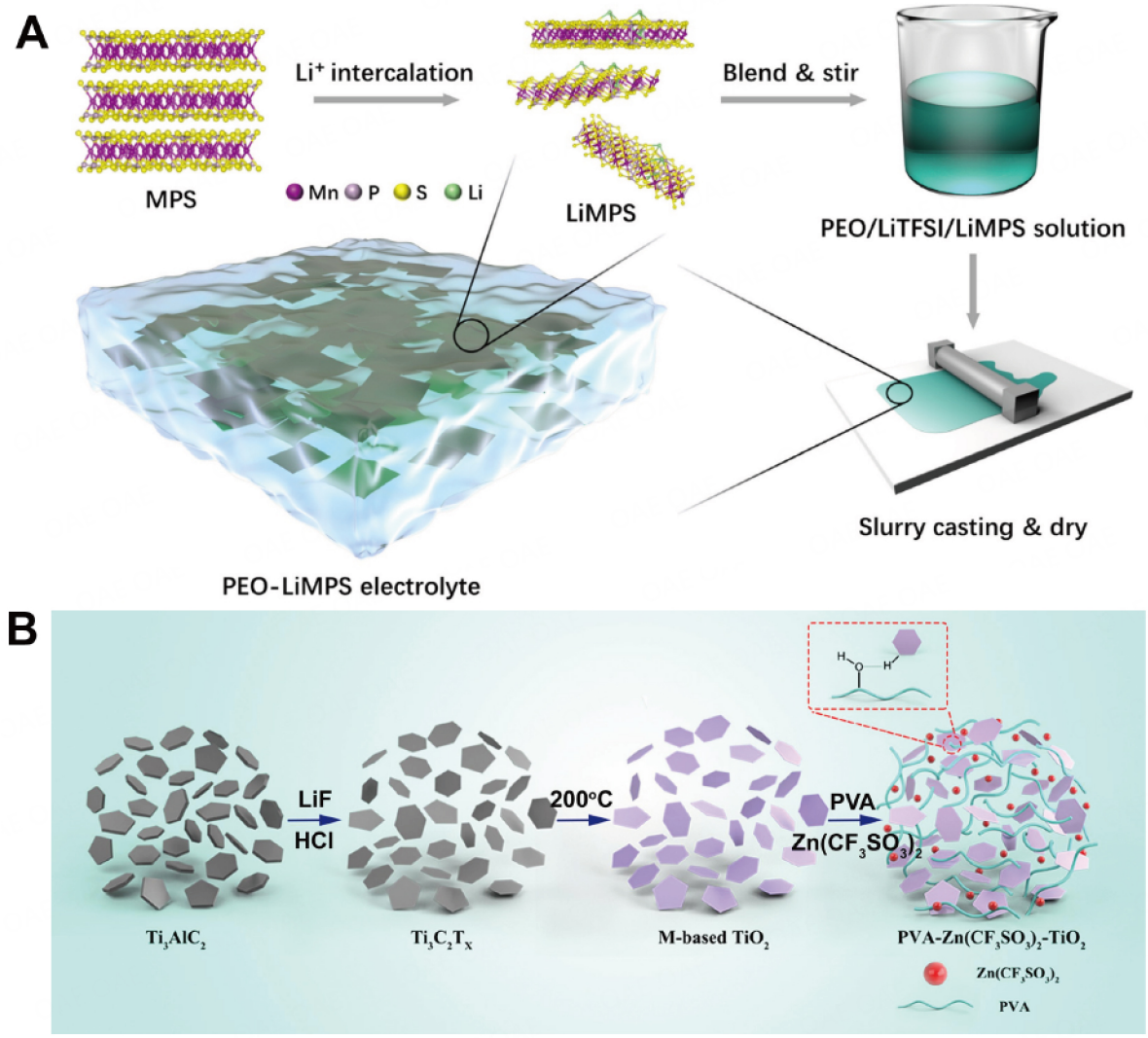

Figure 9. 2D materials as solid electrolyte additive. (A) Illustration of Li^+ intercalation, bulk MPS exfoliation, and the fabrication process of PEO-LiMPS electrolytes. Reproduced with permission[172]. Copyright 2023, Elsevier. (B) Schematic diagrams for the fabrication of TiO_2 nanosheets through in situ HF etching, hydrothermal oxidation, and incorporation with PVA–$Zn(CF_3SO_3)_2$ gel electrolytes. Reproduced with permission[174]. Copyright 2022, Elsevier.

glass fiber (GF) separators in Zn-ion batteries, as displayed in Figure 10C[176]. In addition to acting as physical armor to prevent the separator from being penetrated, the g-C_3N_4 can also induce coordinate interaction between Zn ions and the abundant nitrogen species at the surface of nanosheets, regulating the metal ions flux through the pores of the Janus separators homogeneously. The modified separator demonstrates superior electrochemical performance, with a ten-fold longer lifespan in Zn//Zn symmetrical batteries. Recently, a $Ti_3C_2T_x$ MXene layer combined with a commercial GF separator has been reported, as shown in Figure 10D[177]. By virtue of the high conductive surface with abundant functional groups and the highly matched lattice contact with the Zn anode, the MXene can generate homogeneous surface electric field to achieve uniform zinc$^+$ deposition. Additionally, the intrinsic negatively charged MXene functionalized as an ion sieving to effectively reduce the concentration of SO_4^{2-} and H^+, resulting in the inhibition of side reactions. Superior cycle stability for more than 2500 h and extremely low nucleation overpotential was obtained.

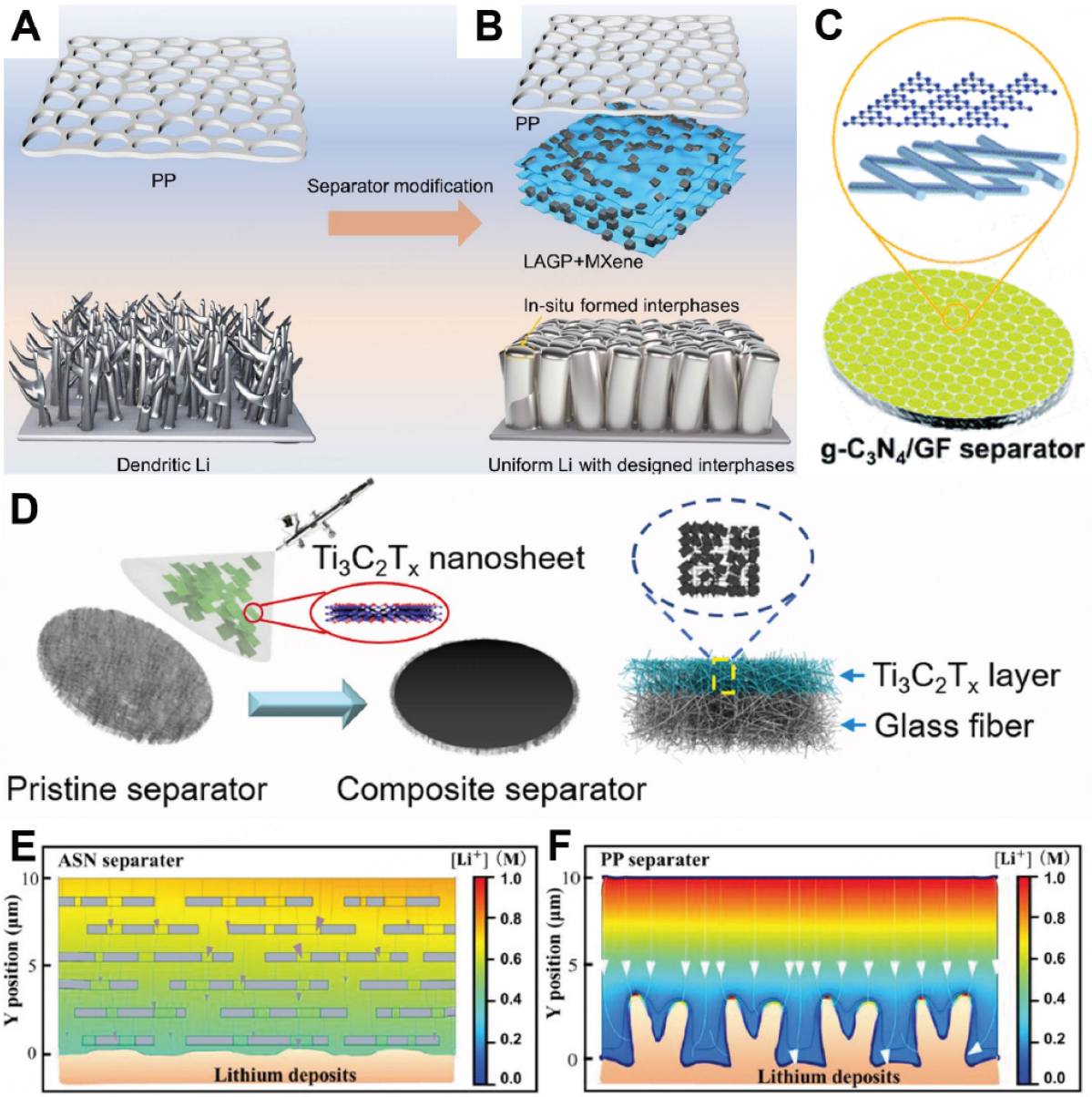

Figure 10. 2D materials for separator. (A, B) Dendritic Li deposition under traditional porous PP separator compared to uniform planar-like Li deposition with designed stable interphases by using the modified separator. Reproduced with permission[175]. Copyright 2021, Elsevier. (C) Schematic of the g-C_3N_4/GF separator, C_3N_4 provides physical protection and coordinates active sites for regulating Zn^{2+} flux. Reproduced with permission[176]. Copyright 2021, Royal Society of Chemistry. (D) Schematics illustrating the design of $Ti_3C_2T_x$ @glass fiber composite separator to stabilize the Zn anode. Reproduced with permission[177]. Copyright 2023, Elsevier. The simulated lithium-ion concentration distribution profiles throughout the (E) ASN-Sep and (F) PP-Sep. The presence of high porosity and abundant surface oxygen groups in ASN separator enables the uniform dispersion of Li-ion flux. Reproduced with permission[178]. Copyright 2023, Wiley-VCH GmbH.

2D materials as ion sieving separator

Due to the various shortcomings of conventional polyolefin separators, including poor wettability to electrolytes, being susceptible to thermal contraction, and poor resistance to mechanical stress and deformation, many attempts have been made to develop novel materials that have higher porosity, better thermal stability, and larger Young's modulus. It was recently reported using clay-originated holey

amorphous silica nanosheets (ASN) for inorganic separators in lithium metal batteries[178]. As shown in Figure 10E and F, the synthesis involved a two-step ion exchange, followed by multiple acid/water wash and purification of the vermiculite crystals. Remarkably, this environmentally friendly process does not use any toxic chemicals, gas, or raw materials. High porosity and abundant surface oxygen groups facilitate the homogeneous distribution of Li-ion flux and promote the dissociation of C-F bonds in the electrolytes, leading to a LiF-rich SEI layer. As a result, superior stability of Li electroplating/stripping for 2000 h was achieved, suggesting good inhibition of dendrite formation and electrolyte consumption. Jiang *et al.*[179] presented a straightforward approach to achieve anisotropic ordering of 2D COFs by depositing them onto graphene to form double-layer membranes as ionic sieves, which effectively suppressed the shuttle effect and demonstrated enhanced cyclability in Li-S batteries. Cao *et al.*[180] have successfully developed a 2D Mn-MOF with angstrom-level ion tunnels that effectively suppress side reactions, leading to an ultra-long lifespan and high performance in zinc anodes, as well as demonstrating potential for other metal anodes.

CONCLUSION AND OUTLOOK

In this review, we summarized recent advancements of various 2D materials. Due to the limitation of current commercial LIBs, the development of metal batteries with high specific energy has become a hot spot. The major challenge of the application of metal batteries is the formation of dendrites. The distinctive traits of 2D materials, such as excellent mechanical strength and flexibility, adjustable electronic properties and controllable assembly features, are beneficial for the dendrite-free metal batteries. We outline the recent strategies for utilizing 2D materials in key components of dendrite-free batteries, including the anode, electrolyte, and separator. These materials also possess high mechanical strength and stability due to their atomic-thin nature, which can help prevent dendrite growth and enhance the durability of the battery. Superior surface area-to-volume ratio and high catalytic activity enhance the performance of the battery and improve energy efficiency. The properties of 2D materials may also be adjusted through various methods, such as doping or functionalization, which can enable the development of customized materials for dendrite-free battery applications. Hereby, we propose future perspectives and potential outlooks for the development of 2D materials in the dendrite-free metal batteries.

Exploring the potential formation mechanism. 2D materials can be used to simulate the behavior of metal anodes at the atomic or molecular scale[144]. By using 2D materials as a model system, researchers can gain insights into the fundamental mechanisms that govern dendrite formation and growth, such as surface diffusion, nucleation, and crystal growth. This can help identify the key factors that contribute to dendrite formation and inform the development of strategies to prevent or mitigate dendrite growth in batteries.

(2) Developing the techniques for in situ/operando observation of dendrite growth. Because 2D materials are easy to exfoliate, researchers can create a platform for observing dendrite formation and growth in real-time from the nanoscale during battery operation. For example, by utilizing a high-flux light source, a synchrotron X-ray absorption spectroscopy (XAS) beamline can conduct qualitative or quantitative analysis towards certain elements, resulting in a deep and effective understanding of electrochemical reaction mechanisms within the battery system. Ni *et al.*[181] used synchrotron X-ray tomography to *in situ* visualize and understand the interaction between separators and potassium dendrite growth, providing valuable insights into the mechanisms of dendrite formation and potential strategies for mitigating dendrite-induced failures in K-ion batteries, as shown in Figure 11A. *In situ* synchrotron XAS allows the real-time monitoring of dynamic changes of electronic and atomic structures in battery operation process. Yu *et al.*[182] utilizing operando X-ray techniques to regulate key variables and visualize the growth of lithium dendrites, providing valuable insights into the mechanisms and factors influencing dendrite formation. The schematic illustration of *operando* X-ray imaging techniques is displayed in Figure 11B. These changes can be divided

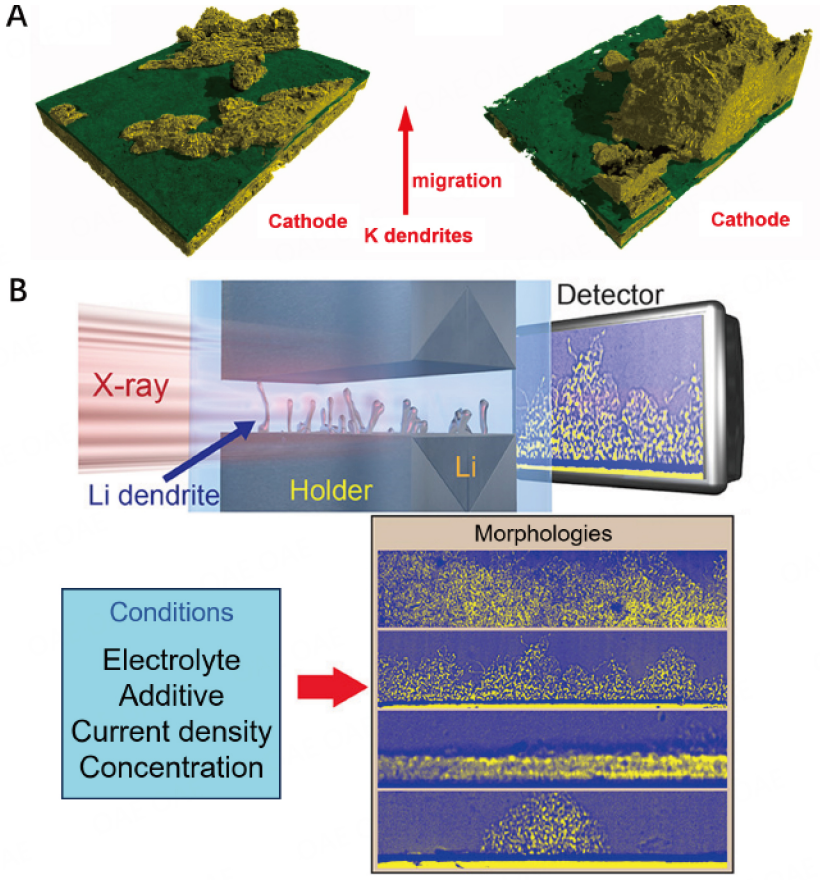

Figure 11. *In situ* measurement. (A) Three dimensional reconstructed volumes of potassium dendrite growth via *in situ* synchrotron X-ray tomography. Reproduced with permission[181]. Copyright 2021, Elsevier. (B) Schematic illustration of *operando* X-ray imaging techniques to observe the deposition and stripping of lithium metal under real-world battery operations. Reproduced with permission[182]. Copyright 2019, American Chemical Society.

into valence state change, local geometry and symmetry change, charge transfer and number/length/type change of chemical bonds[183]. An *in situ* transmission electron microscope (TEM) is a promising tool for visualizing the nucleating and plating behavior on the electrode surface from the nanoscale in real time. During the process, the selected area diffraction (SAED) patterns can also be obtained before and after plating to study the phase transformation of the electrode. Our group first reported the nucleation and deposition behavior on the graphene surface at the nanoscale and compared it with that on the SnSe-modified graphene[154]. These techniques can establish atomic and fundamental structure-performance relationships between 2D materials and metal batteries. On the other hand, 2D materials offer several advantages that enable the development of in situ/operando observation of dendrite growth. Firstly, their ultrathin nature allows for direct visualization of the underlying interfaces and dendrite structures. Their excellent electrical and thermal conductivity facilitates accurate monitoring of electrochemical processes and temperature changes during dendrite growth. Additionally, the large surface area-to-volume ratio and chemical stability enable long-term in situ observation.

Constructing new battery systems including flexible and wearable batteries and solid-state batteries. Considering that 2D materials possess mechanical flexibility and can be synthesized into thin films, they emerge as promising candidates for flexible and wearable batteries. By developing new battery systems based on these materials, flexible and lightweight batteries can be achieved and integrated into a broad

spectrum of wearable and portable devices[184,185]. Additionally, 2D materials hold promise for the development of solid-state batteries for their high ionic conductivity and stability[186]. Solid-state batteries have the potential to provide enhanced safety, higher energy density, wider temperature range, and faster charging capabilities[187]. However, several challenges need to be addressed, including achieving high ionic conductivity in solid electrolytes, ensuring stable interfaces, controlling dendrite formation, and identifying scalable materials[188,189]. The practical utilization of solid-state batteries can experience remarkable enhancements through the incorporation of 2D materials. By harnessing the high ionic conductivity and stability of novel 2D materials and advanced fabrication methods, the scope of 2D material application in solid-state batteries can be expanded. This expansion holds the promise of enhancing battery performance and promoting wider acceptance of solid-state batteries across diverse applications.

In summary, recent work provides deep insights on how to design dendrite-free metal batteries with various 2D materials. These findings can aid in the development of more comprehensive metal anodes for next-generation high-performance metal batteries.

DECLARATIONS

Authors' contributions

Conceptualization, investigation, writing - original draft: Xu M, Xin Z
Literature survey - revision: Wang J, Tang TW, Li Y, Li Y, Kim TH
Review & editing, supervision: Luo Z

Availability of data and materials

Not applicable.

Financial support and sponsorship

The work described in this paper was partially supported by a grant from the Research Grants Council of the Hong Kong Special Administrative Region, China (Project No. HKUST C6008-20E, 16304421), Research Fund of Guangdong-Hong Kong-Macao Joint Laboratory for Intelligent Micro-Nano Optoelectronic Technology (2020B1212030010), and Shenzhen Special Fund for Central Guiding the Local Science and Technology Development (2021Szvup136).

Conflicts of interest

All authors declared that there are no conflicts of interest.

Ethical approval and consent to participate

Not applicable

Consent for publication

Not applicable.

REFERENCES

1. Han X, Gong Y, Fu KK, et al. Negating interfacial impedance in garnet-based solid-state Li metal batteries. *Nat Mater* 2017;16:572-9. DOI
2. Chen C, Zhang Y, Li Y, et al. Highly conductive, lightweight, low-tortuosity carbon frameworks as ultrathick 3D current collectors. *Adv Energy Mater* 2017;7:1700595. DOI
3. Zhang B, Kang F, Tarascon J, Kim J. Recent advances in electrospun carbon nanofibers and their application in electrochemical

energy storage. *Prog Mater Sci* 2016;76:319-80. DOI
4. Bae S, Kim H, Lee Y, et al. Roll-to-roll production of 30-inch graphene films for transparent electrodes. *Nat Nanotechnol* 2010;5:574-8. DOI
5. Kaltenbrunner M, Sekitani T, Reeder J, et al. An ultra-lightweight design for imperceptible plastic electronics. *Nature* 2013;499:458-63. DOI
6. Cao Q, Rogers JA. Ultrathin films of single-walled carbon nanotubes for electronics and sensors: a review of fundamental and applied aspects. *Adv Mater* 2009;21:29-53. DOI
7. Kasavajjula U, Wang C, Appleby AJ. Nano- and bulk-silicon-based insertion anodes for lithium-ion secondary cells. *J Power Sources* 2007;163:1003-39. DOI
8. Xu Z, Liu X, Luo Y, Zhou L, Kim J. Nanosilicon anodes for high performance rechargeable batteries. *Prog Mater Sci* 2017;90:1-44. DOI
9. Placke T, Kloepsch R, Dühnen S, Winter M. Lithium ion, lithium metal, and alternative rechargeable battery technologies: the odyssey for high energy density. *J Solid State Electrochem* 2017;21:1939-64. DOI
10. Li M, Lu J, Chen Z, Amine K. 30 years of lithium-ion batteries. *Adv Mater* 2018:e1800561. DOI
11. Ding Y, Cano ZP, Yu A, Lu J, Chen Z. Automotive Li-Ion batteries: current status and future perspectives. *Electrochem Energ Rev* 2019;2:1-28. DOI
12. Yuan H, Ding X, Liu T, et al. A review of concepts and contributions in lithium metal anode development. *Mater Today* 2022;53:173-96. DOI
13. Lu G, Nai J, Luan D, Tao X, Lou XWD. Surface engineering toward stable lithium metal anodes. *Sci Adv* 2023;9:eadf1550. DOI PubMed PMC
14. Chu C, Li R, Cai F, et al. Recent advanced skeletons in sodium metal anodes. *Energy Environ Sci* 2021;14:4318-40. DOI
15. Wang T, Hua Y, Xu Z, Yu JS. Recent advanced development of artificial interphase engineering for stable sodium metal anodes. *Small* 2022;18:e2102250. DOI
16. Ma L, Cui J, Yao S, et al. Dendrite-free lithium metal and sodium metal batteries. *Energ Storage Mater* 2020;27:522-54. DOI
17. Liu P, Mitlin D. Emerging potassium metal anodes: perspectives on control of the electrochemical interfaces. *Acc Chem Res* 2020;53:1161-75. DOI PubMed
18. Wei C, Tao Y, Fei H, et al. Recent advances and perspectives in stable and dendrite-free potassium metal anodes. *Energ Storage Mater* 2020;30:206-27. DOI
19. Yi Z, Chen G, Hou F, Wang L, Liang J. Strategies for the stabilization of zn metal anodes for Zn-Ion batteries. *Adv Energy Mater* 2021;11:2003065. DOI
20. Li C, Xie X, Liang S, Zhou J. Issues and future perspective on zinc metal anode for rechargeable aqueous zinc-ion batteries. *Energ Environ Mater* 2020;3:146-59. DOI
21. Niu J, Zhang Z, Aurbach D. Alloy anode materials for rechargeable Mg ion batteries. *Adv Energy Mater* 2020;10:2000697. DOI
22. Jiang J, Liu J. Iron anode-based aqueous electrochemical energy storage devices: Recent advances and future perspectives. *Interdiscip Mater* 2022;1:116-39. DOI
23. Jiang M, Fu C, Meng P, et al. Challenges and strategies of low-cost aluminum anodes for high-performance Al-based batteries. *Adv Mater* 2022;34:e2102026. DOI
24. Wu F, Yang H, Bai Y, Wu C. Paving the path toward reliable cathode materials for aluminum-ion batteries. *Adv Mater* 2019;31:e1806510. DOI
25. Yang H, Li H, Li J, et al. The rechargeable aluminum battery: opportunities and challenges. *Angew Chem Int Ed Engl* 2019;58:11978-96. DOI
26. Wei C, Tan L, Zhang Y, et al. Covalent Organic Frameworks and Their Derivatives for Better Metal Anodes in Rechargeable Batteries. *ACS Nano* 2021;15:12741-67. DOI
27. Rosenman A, Markevich E, Salitra G, Aurbach D, Garsuch A, Chesneau FF. Review on Li-sulfur battery systems: an integral perspective. *Adv Energy Mater* 2015;5:1500212. DOI
28. Luo C, Zhu Y, Borodin O, et al. Activation of oxygen-stabilized sulfur for Li and Na batteries. *Adv Funct Materials* 2016;26:745-52. DOI
29. Zhou C, Lu K, Zhou S, et al. Strategies toward anode stabilization in nonaqueous alkali metal-oxygen batteries. *Chem Commun (Camb)* 2022;58:8014-24. DOI
30. Wu C, Lou J, Zhang J, et al. Current status and future directions of all-solid-state batteries with lithium metal anodes, sulfide electrolytes, and layered transition metal oxide cathodes. *Nano Energy* 2021;87:106081. DOI
31. Zhang H, Sun C. Cost-effective iron-based aqueous redox flow batteries for large-scale energy storage application: a review. *J Power Sources* 2021;493:229445. DOI
32. Li B, Liu J. Progress and directions in low-cost redox-flow batteries for large-scale energy storage. *Nat Sci Rev* 2017;4:91-105. DOI
33. Nie W, Cheng H, Sun Q, et al. Design Strategies toward high-performance Zn metal anode. *Small Methods* 2023:e2201572. DOI
34. Fan L, Li X. Recent advances in effective protection of sodium metal anode. *Nano Energy* 2018;53:630-42. DOI
35. Xu M, Li Y, Ihsan-ul-haq M, et al. NaF-rich solid electrolyte interphase for dendrite-free sodium metal batteries. *Energ Storage Mater* 2022;44:477-86. DOI
36. Zhang Y, Zuo T, Popovic J, et al. Towards better Li metal anodes: challenges and strategies. *Mater Today* 2020;33:56-74. DOI

37. Han Y, Liu B, Xiao Z, et al. Interface issues of lithium metal anode for high-energy batteries: Challenges, strategies, and perspectives. *InfoMat* 2021;3:155-74. DOI
38. Zhang X, Lv R, Tang W, et al. Challenges and opportunities for multivalent metal anodes in rechargeable batteries. *Adv Funct Materials* 2020;30:2004187. DOI
39. Chen Y, Luo Y, Zhang H, Qu C, Zhang H, Li X. The challenge of lithium metal anodes for practical applications. *Small Methods* 2019;3:1800551. DOI
40. Zheng X, Bommier C, Luo W, Jiang L, Hao Y, Huang Y. Sodium metal anodes for room-temperature sodium-ion batteries: Applications, challenges and solutions. *Energy Storage Mater* 2019;16:6-23. DOI
41. Du W, Ang EH, Yang Y, Zhang Y, Ye M, Li CC. Challenges in the material and structural design of zinc anode towards high-performance aqueous zinc-ion batteries. *Energy Environ Sci* 2020;13:3330-60. DOI
42. Brissot C, Rosso M, Chazalviel J, Baudry P, Lascaud S. In situ study of dendritic growth inlithium/PEO-salt/lithium cells. *Electrochim Acta* 1998;43:1569-74. DOI
43. Rosso M, Gobron T, Brissot C, Chazalviel J, Lascaud S. Onset of dendritic growth in lithium/polymer cells. *J Power Sources* 2001;97-98:804-6. DOI
44. Zhang R, Cheng XB, Zhao CZ, et al. Conductive nanostructured scaffolds render low local current density to inhibit lithium dendrite growth. *Adv Mater* 2016;28:2155-62. DOI
45. Zhang Y, Liu B, Hitz E, et al. A carbon-based 3D current collector with surface protection for Li metal anode. *Nano Res* 2017;10:1356-65. DOI
46. Brissot C, Rosso M, Chazalviel J-, Lascaud S. In situ concentration cartography in the neighborhood of dendrites growing in lithium/polymer-electrolyte/lithium cells. *J Electrochem Soc* 1999;146:4393-400. DOI
47. Brissot C, Rosso M, Chazalviel J, Lascaud S. Dendritic growth mechanisms in lithium/polymer cells. *J Power Sources* 1999;81-82:925-9. DOI
48. Zhang Y, Yao Y, Sendeku MG, et al. Recent progress in CVD growth of 2D transition metal dichalcogenides and related heterostructures. *Adv Mater* 2019;31:e1901694. DOI
49. Zavabeti A, Jannat A, Zhong L, Haidry AA, Yao Z, Ou JZ. Two-dimensional materials in large-areas: synthesis, properties and applications. *Nanomicro Lett* 2020;12:66. DOI PubMed PMC
50. Mannix AJ, Kiraly B, Hersam MC, Guisinger NP. Synthesis and chemistry of elemental 2D materials. *Nat Rev Chem* 2017:1. DOI
51. Rojaee R, Shahbazian-Yassar R. Two-dimensional materials to address the lithium battery challenges. *ACS Nano* 2020;14:2628-58. DOI PubMed
52. Wei C, Tao Y, An Y, et al. Recent advances of emerging 2D mxene for stable and dendrite-free metal anodes. *Adv Funct Materials* 2020;30:2004613. DOI
53. Zheng S, Zhao W, Chen J, Zhao X, Pan Z, Yang X. 2D materials boost advanced Zn anodes: principles, advances, and challenges. *Nanomicro Lett* 2023;15:46. DOI PubMed PMC
54. Li Z, Zhang Y, Guan H, et al. Rationally integrating 2D confinement and high sodiophilicity toward SnO(2)/Ti(3) C(2) T(x) composites for high-performance sodium-metal anodes. *Small* 2023;19:e2208277. DOI
55. Cao Z, Zhang Y, Cui Y, et al. Harnessing the unique features of 2D materials toward dendrite-free metal anodes. *Energy Environ Mater* 2022;5:45-67. DOI
56. Bunch JS, Verbridge SS, Alden JS, et al. Impermeable atomic membranes from graphene sheets. *Nano Lett* 2008;8:2458-62. DOI
57. Lee C, Wei X, Kysar JW, Hone J. Measurement of the elastic properties and intrinsic strength of monolayer graphene. *Science* 2008;321:385-8. DOI
58. Nair RR, Blake P, Grigorenko AN, et al. Fine structure constant defines visual transparency of graphene. *Science* 2008;320:1308. DOI
59. Bolotin KI, Jiang Z, Klima M, Fudenberg G, Hone J, Kim P, Stormer HL. Ultrahigh electron mobility in suspended graphene. *Solid State Commun* 2008;146:351. DOI
60. Su CY, Lu AY, Xu Y, Chen FR, Khlobystov AN, Li LJ. High-quality thin graphene films from fast electrochemical exfoliation. *ACS Nano* 2011;5:2332-9. DOI PubMed
61. Muñoz R, Gómez-aleixandre C. Review of CVD synthesis of graphene. *Chem Vap Deposition* 2013;19:297-322. DOI
62. Vazirisereshk MR, Hasz K, Zhao MQ, Johnson ATC, Carpick RW, Martini A. Nanoscale friction behavior of transition-metal dichalcogenides: role of the chalcogenide. *ACS Nano* 2020;14:16013-21. DOI PubMed
63. Zong X, Yan H, Wu G, et al. Enhancement of photocatalytic H_2 evolution on CdS by loading MoS_2 as Cocatalyst under visible light irradiation. *J Am Chem Soc* 2008;130:7176-7. DOI
64. Liu Y, Guo J, Zhu E, et al. Approaching the Schottky-Mott limit in van der Waals metal-semiconductor junctions. *Nature* 2018;557:696-700. DOI
65. Sun G, Li B, Li J, et al. Direct van der Waals epitaxial growth of 1D/2D Sb_2Se_3/WS_2 mixed-dimensional p-n heterojunctions. *Nano Res* 2019;12:1139-45. DOI
66. Wang X, Lin J, Zhu Y, et al. Chemical vapor deposition of trigonal prismatic NbS(2) monolayers and 3R-polytype few-layers. *Nanoscale* 2017;9:16607-11. DOI
67. Deng Y, Lai Y, Zhao X, et al. Controlled Growth of 3R Phase Tantalum Diselenide and Its Enhanced Superconductivity. *J Am Chem Soc* 2020;142:2948-55. DOI

68. Acerce M, Voiry D, Chhowalla M. Metallic 1T phase MoS2 nanosheets as supercapacitor electrode materials. *Nat Nanotechnol* 2015;10:313-8. DOI PubMed
69. Liu Z, Ou X, Zhuang M, et al. Confinement-enhanced rapid interlayer diffusion within graphene-supported anisotropic ReSe(2) electrodes. *ACS Appl Mater Interfaces* 2019;11:31147-54. DOI
70. Liu Z, Daali A, Xu GL, et al. Highly reversible sodiation/desodiation from a carbon-sandwiched snS(2) nanosheet anode for sodium ion batteries. *Nano Lett* 2020;20:3844-51. DOI
71. Kim SY, Kwak J, Ciobanu CV, Kwon SY. Recent developments in controlled vapor-phase growth of 2D group 6 transition metal dichalcogenides. *Adv Mater* 2019;31:e1804939. DOI PubMed
72. Wang F, Tu B, He P, et al. Uncovering the conduction behavior of van der waals ambipolar semiconductors. *Adv Mater* 2019;31:e1805317. DOI
73. Chen Y, Peng B, Cong C, et al. In-Plane Anisotropic Thermal conductivity of few-layered transition metal dichalcogenide Td-WTe(2). *Adv Mater* 2019;31:e1804979. DOI
74. Zhu C, Chen Y, Liu F, et al. Light-tunable 1T-TaS(2) charge-density-wave oscillators. *ACS Nano* 2018;12:11203-10. DOI
75. Bosi M. Growth and synthesis of mono and few-layers transition metal dichalcogenides by vapour techniques: a review. *RSC Adv* 2015;5:75500-18. DOI
76. Zhang K, Feng Y, Wang F, Yang Z, Wang J. Two dimensional hexagonal boron nitride (2D-hBN): synthesis, properties and applications. *J Mater Chem C* 2017;5:11992-2022. DOI
77. Costa C, Barbosa J, Gonçalves R, Castro H, Campo FD, Lanceros-méndez S. Recycling and environmental issues of lithium-ion batteries: Advances, challenges and opportunities. *Energ Storage Mater* 2021;37:433-65. DOI
78. Chen TA, Chuu CP, Tseng CC, et al. Wafer-scale single-crystal hexagonal boron nitride monolayers on Cu (111). *Nature* 2020;579:219-23. DOI
79. Ma KY, Zhang L, Jin S, et al. Epitaxial single-crystal hexagonal boron nitride multilayers on Ni (111). *Nature* 2022;606:88-93. DOI
80. Kim KK, Hsu A, Jia X, et al. Synthesis of monolayer hexagonal boron nitride on Cu foil using chemical vapor deposition. *Nano Lett* 2012;12:161-6. DOI
81. Kim SM, Hsu A, Park MH, et al. Synthesis of large-area multilayer hexagonal boron nitride for high material performance. *Nat Commun* 2015;6:8662. DOI PubMed PMC
82. Zeng F, Wang R, Wei W, et al. Stamped production of single-crystal hexagonal boron nitride monolayers on various insulating substrates. *Nat Commun* 2023;14:6421. DOI PubMed PMC
83. Singhal R, Echeverria E, Mcilroy DN, Singh RN. Synthesis of hexagonal boron nitride films on silicon and sapphire substrates by low-pressure chemical vapor deposition. *Thin Solid Films* 2021;733:138812. DOI
84. Mehek R, Iqbal N, Noor T, et al. Metal-organic framework based electrode materials for lithium-ion batteries: a review. *RSC Adv* 2021;11:29247-66. DOI PubMed PMC
85. Liu X, Jin Y, Wang H, et al. In situ growth of covalent organic framework nanosheets on graphene as the cathode for long-life high-capacity lithium-ion batteries. *Adv Mater* 2022;34:e2203605. DOI
86. Kong L, Liu M, Huang H, Xu Y, Bu X. Metal/covalent-organic framework based cathodes for metal-ion batteries. *Adv Energy Mater* 2022;12:2100172. DOI
87. Cravillon J, Münzer S, Lohmeier S, Feldhoff A, Huber K, Wiebcke M. Rapid room-temperature synthesis and characterization of nanocrystals of a prototypical zeolitic imidazolate framework. *Chem Mater* 2009;21:1410-2. DOI
88. Chui SS, Lo SM, Charmant JP, Orpen AG, Williams ID. A chemically functionalizable nanoporous material. *Science* 1999;283:1148-50. DOI PubMed
89. Tranchemontagne DJ, Hunt JR, Yaghi OM. Room temperature synthesis of metal-organic frameworks: MOF-5, MOF-74, MOF-177, MOF-199, and IRMOF-0. *Tetrahedron* 2008;64:8553-7. DOI
90. Stock N, Biswas S. Synthesis of metal-organic frameworks (MOFs): routes to various MOF topologies, morphologies, and composites. *Chem Rev* 2012;112:933-69. DOI PubMed
91. Campbell NL, Clowes R, Ritchie LK, Cooper AI. Rapid microwave synthesis and purification of porous covalent organic frameworks. *Chem Mater* 2009;21:204-6. DOI
92. Biswal BP, Chandra S, Kandambeth S, Lukose B, Heine T, Banerjee R. Mechanochemical synthesis of chemically stable isoreticular covalent organic frameworks. *J Am Chem Soc* 2013;135:5328-31. DOI PubMed
93. Kim S, Park C, Lee M, et al. Rapid Photochemical synthesis of sea-urchin-shaped hierarchical porous COF-5 and its lithography-free patterned growth. *Adv Funct Materials* 2017;27:1700925. DOI
94. Ren H, Wei T. Electrochemical synthesis methods of metal-organic frameworks and their environmental analysis applications: a review. *ChemElectroChem* 2022;9:e202200196. DOI
95. Zhang M, Chen J, Zhang S, et al. Electron beam irradiation as a general approach for the rapid synthesis of covalent organic frameworks under ambient conditions. *J Am Chem Soc* 2020;142:9169-74. DOI
96. Alhabeb M, Maleski K, Anasori B, et al. Guidelines for synthesis and processing of two-dimensional titanium carbide (Ti_3C_2Tx MXene). *Chem Mater* 2017;29:7633-44. DOI
97. Sang X, Xie Y, Lin MW, et al. Atomic defects in monolayer titanium carbide (Ti(3)C(2)T(x)) MXene. *ACS Nano* 2016;10:9193-200. DOI
98. Guo Z, Zhou J, Si C, Sun Z. Flexible two-dimensional Tin+1Cn (n = 1, 2 and 3) and their functionalized MXenes predicted by

density functional theories. *Phys Chem Chem Phys* 2015;17:15348-54. DOI PubMed

99. Hart JL, Hantanasirisakul K, Lang AC, et al. Control of MXenes' electronic properties through termination and intercalation. *Nat Commun* 2019;10:522. DOI PubMed PMC
100. Jiang Y, Sun T, Xie X, et al. Oxygen-functionalized ultrathin Ti(3)C(2)T(x) MXene for enhanced electrocatalytic hydrogen evolution. *ChemSusChem* 2019;12:1368-73. DOI
101. Naguib M, Kurtoglu M, Presser V, et al. Two-dimensional nanocrystals produced by exfoliation of Ti3 AlC2. *Adv Mater* 2011;23:4248-53. DOI
102. Zhan X, Si C, Zhou J, Sun Z. MXene and MXene-based composites: synthesis, properties and environment-related applications. *Nanoscale Horiz* 2020;5:235-58. DOI
103. Anasori B, Xie Y, Beidaghi M, et al. Two-Dimensional, ordered, double transition metals carbides (MXenes). *ACS Nano* 2015;9:9507-16. DOI
104. Li Y, Shao H, Lin Z, et al. A general Lewis acidic etching route for preparing MXenes with enhanced electrochemical performance in non-aqueous electrolyte. *Nat Mater* 2020;19:894-9. DOI
105. Yang S, Zhang P, Wang F, et al. Fluoride-free synthesis of two-dimensional titanium carbide (MXene) using a binary aqueous system. *Angew Chem Int Ed Engl* 2018;57:15491-5. DOI
106. Li T, Yao L, Liu Q, et al. Fluorine-free synthesis of high-purity Ti(3)C(2)T(x) (T=OH, O) via alkali treatment. *Angew Chem Int Ed Engl* 2018;57:6115-9. DOI
107. Wang D, Zhou C, Filatov AS, et al. Direct synthesis and chemical vapor deposition of 2D carbide and nitride MXenes. *Science* 2023;379:1242-7. DOI
108. Liu J, Liu XW. Two-dimensional nanoarchitectures for lithium storage. *Adv Mater* 2012;24:4097-111. DOI PubMed
109. Sun W, Rui X, Zhu J, et al. Ultrathin nickel oxide nanosheets for enhanced sodium and lithium storage. *J Power Sources* 2015;274:755-61. DOI
110. Zhang X, Shi W, Zhu J, et al. Synthesis of porous NiO nanocrystals with controllable surface area and their application as supercapacitor electrodes. *Nano Res* 2010;3:643-52. DOI
111. Garg N, Basu M, Ganguli AK. Nickel cobaltite nanostructures with enhanced supercapacitance activity. *J Phys Chem C* 2014;118:17332-41. DOI
112. Jiang H, Zhao T, Li C, Ma J. Hierarchical self-assembly of ultrathin nickel hydroxide nanoflakes for high-performance supercapacitors. *J Mater Chem* 2011;21:3818. DOI
113. Kurra N, Alhebshi NA, Alshareef HN. Microfabricated pseudocapacitors using $Ni(OH)_2$ electrodes exhibit remarkable volumetric capacitance and energy density. *Advanced Energy Materials* 2015;5:1401303. DOI
114. Yang GW, Xu CL, Li HL. Electrodeposited nickel hydroxide on nickel foam with ultrahigh capacitance. *Chem Commun (Camb)* 2008:6537-9. DOI PubMed
115. Xia F, Wang H, Jia Y. Rediscovering black phosphorus as an anisotropic layered material for optoelectronics and electronics. *Nat Commun* 2014;5:4458. DOI
116. Qiao J, Kong X, Hu ZX, Yang F, Ji W. High-mobility transport anisotropy and linear dichroism in few-layer black phosphorus. *Nat Commun* 2014;5:4475. DOI PubMed PMC
117. Li L, Yang F, Ye GJ, et al. Quantum Hall effect in black phosphorus two-dimensional electron system. *Nat Nanotechnol* 2016;11:593-7. DOI
118. Luo Z, Maassen J, Deng Y, et al. Anisotropic in-plane thermal conductivity observed in few-layer black phosphorus. *Nat Commun* 2015;6:8572. DOI PubMed PMC
119. Guo Z, Zhang H, Lu S, et al. From black phosphorus to phosphorene: basic solvent exfoliation, evolution of raman scattering, and applications to ultrafast photonics. *Adv Funct Materials* 2015;25:6996-7002. DOI
120. Pei J, Gai X, Yang J, et al. Producing air-stable monolayers of phosphorene and their defect engineering. *Nat Commun* 2016;7:10450. DOI PubMed PMC
121. Gao J, Zhang G, Zhang YW. The critical role of substrate in stabilizing phosphorene nanoflake: a theoretical exploration. *J Am Chem Soc* 2016;138:4763-71. DOI PubMed
122. Wong H, Li Y, Wang J, et al. Two-dimensional materials for high density, safe and robust metal anodes batteries. *Nano Converg* 2023;10:37. DOI PubMed PMC
123. Zhang C, Wang A, Zhang J, Guan X, Tang W, Luo J. 2D Materials for lithium/sodium metal anodes. *Adv Energy Mater* 2018;8:1802833. DOI
124. Shang M, Shovon OG, Wong FEY, Niu J. A BF(3) -doped MXene dual-layer interphase for a reliable lithium-metal anode. *Adv Mater* 2023;35:e2210111. DOI PubMed
125. Han KH, Seok JY, Kim IH, et al. A 2D ultrathin nanopatterned interlayer to suppress lithium dendrite growth in high-energy lithium-metal anodes. *Adv Mater* 2022;34:e2203992. DOI
126. Zhou J, Xie M, Wu F, et al. Ultrathin surface coating of nitrogen-doped graphene enables stable zinc anodes for aqueous zinc-ion batteries. *Adv Mater* 2021;33:e2101649. DOI
127. Jiang Z, Liu T, Yan L, et al. Metal-organic framework nanosheets-guided uniform lithium deposition for metallic lithium batteries. *Energ Storage Mater* 2018;11:267-73. DOI
128. Landsman MR, Sujanani R, Brodfuehrer SH, et al. Water treatment: are membranes the panacea? *Annu Rev Chem Biomol Eng*

2020;11:559-85. DOI

129. Denny MS, Moreton JC, Benz L, Cohen SM. Metal–organic frameworks for membrane-based separations. *Nat Rev Mater* 2016:1. DOI
130. Zhang Y, Li J, Zhao W, et al. Defect-free metal-organic framework membrane for precise ion/solvent separation toward highly stable magnesium metal anode. *Adv Mater* 2022;34:e2108114. DOI
131. Zhao F, Zhai P, Wei Y, et al. Constructing artificial sei layer on lithiophilic MXene surface for high-performance lithium metal anodes. *Adv Sci (Weinh)* 2022;9:e2103930. DOI PubMed PMC
132. Zhang D, Wang S, Li B, Gong Y, Yang S. Horizontal growth of lithium on parallelly aligned mxene layers towards dendrite-free metallic lithium anodes. *Adv Mater* 2019;31:e1901820. DOI
133. Cha E, Patel MD, Park J, et al. 2D MoS(2) as an efficient protective layer for lithium metal anodes in high-performance Li-S batteries. *Nat Nanotechnol* 2018;13:337-44. DOI
134. Zhao W, Cao Z, Bayhan Z, et al. A two-dimensional cation-deficient $Ti_{0.87}O_2$ artificial protection layer for stable sodium metal anodes. *Materials Today Energy* 2023;34:101271. DOI
135. Tian Y, An Y, Yang Y, Xu B. Robust nitrogen/selenium engineered MXene/ZnSe hierarchical multifunctional interfaces for dendrite-free zinc-metal batteries. *Energ Storage Mater* 2022;49:122-34. DOI
136. Zhang X, Weng H, Miu Y, et al. Atomic-scale inorganic carbon additive with rich surface polarity and low lattice mismatch for zinc to boost Zn metal anode reversibility. *Chem Eng J* 2024;482:148807. DOI
137. Yang M, Mo Y. Interfacial defect of lithium metal in solid-state batteries. *Angew Chem Int Ed Engl* 2021;60:21494-501. DOI PubMed
138. Liu J, Zhang J, Zhang Z, et al. Epitaxial electrocrystallization of magnesium via synergy of magnesiophilic interface, lattice matching, and electrostatic confinement. *ACS Nano* 2022;16:9894-907. DOI
139. Wang J, Zhang J, Wu J, et al. Interfacial "single-atom-in-defects" catalysts accelerating Li(+) desolvation kinetics for long-lifespan lithium-metal batteries. *Adv Mater* 2023;35:e2302828. DOI
140. Li Y, Min Y, Liang J, et al. Lithiophilic diffusion barrier layer on stainless steel mesh for dendrite suppression and stable lithium metal anode. *Appl Mater Today* 2021;22:100896. DOI
141. Wu Y, Yu Y. 2D material as anode for sodium ion batteries: Recent progress and perspectives. *Energ Storage Mater* 2019;16:323-43. DOI
142. Tian H, Liang J, Liu J. Nanoengineering carbon spheres as nanoreactors for sustainable energy applications. *Adv Mater* 2019;31:e1903886. DOI
143. Tian H, Song A, Tian H, et al. Single-atom catalysts for high-energy rechargeable batteries. *Chem Sci* 2021;12:7656-76. DOI PubMed PMC
144. Li Y, Wong H, Wang J, et al. Deposition of horizontally stacked Zn crystals on single layer 1T-VSe_2 for dendrite-free Zn metal anodes. *Adv Energy Mater* 2022;12:2202983. DOI
145. Zheng J, Zhao Q, Tang T, et al. Reversible epitaxial electrodeposition of metals in battery anodes. *Science* 2019;366:645-8. DOI
146. Wang Y, Xu X, Yin J, et al. MoS(2) -Mediated epitaxial plating of Zn metal anodes. *Adv Mater* 2023;35:e2208171. DOI
147. Wang C, Zheng Z, Feng Y, Ye H, Cao F, Guo Z. Topological design of ultrastrong MXene paper hosted Li enables ultrathin and fully flexible lithium metal batteries. *Nano Energy* 2020;74:104817. DOI
148. Wang T, Liu Y, Lu Y, Hu Y, Fan L. Dendrite-free Na metal plating/stripping onto 3D porous Cu hosts. *Energ Storage Mater* 2018;15:274-81. DOI
149. Zhang S, Xiao S, Li D, et al. Commercial carbon cloth: an emerging substrate for practical lithium metal batteries. *Energ Storage Mater* 2022;48:172-90. DOI
150. Yang H, Zhang L, Wang H, et al. Regulating Na deposition by constructing a Au sodiophilic interphase on CNT modified carbon cloth for flexible sodium metal anode. *J Colloid Interface Sci* 2022;611:317-26. DOI
151. Zhao Y, Sun Q, Li X, et al. Carbon paper interlayers: a universal and effective approach for highly stable Li metal anodes. *Nano Energy* 2018;43:368-75. DOI
152. Lu Z, Zhang Z, Chen X, et al. Improving Li anode performance by a porous 3D carbon paper host with plasma assisted sponge carbon coating. *Energ Storage Mater* 2018;11:47-56. DOI
153. Chen Q, Wei Y, Zhang X, et al. Vertically aligned mxene nanosheet arrays for high-rate lithium metal anodes. *Adv Energy Mater* 2022;12:2200072. DOI
154. Xu M, Liu Z, Li Y, et al. Uniform SnSe nanoparticles on 3D graphene host enabling a dual-nucleation-site interface for dendrite-free sodium metal batteries. *Energ Storage Mater* 2023;60:102848. DOI
155. Shi H, Dong Y, Zheng S, Dong C, Wu ZS. Three dimensional Ti(3)C(2) MXene nanoribbon frameworks with uniform potassiophilic sites for the dendrite-free potassium metal anodes. *Nanoscale Adv* 2020;2:4212-9. DOI PubMed PMC
156. Yan J, Zhi G, Kong D, et al. 3D printed rGO/CNT microlattice aerogel for a dendrite-free sodium metal anode. *J Mater Chem A* 2020;8:19843-54. DOI
157. Yang H, Wang H, Li W, et al. A simple and effective host for sodium metal anode: a 3D-printed high pyrrolic-N doped graphene microlattice aerogel. *J Mater Chem A* 2022;10:16842-52. DOI
158. Wang Z, Huang Z, Wang H, et al. 3D-Printed sodiophilic V(2)CT(x)/rGO-CNT MXene microgrid aerogel for stable Na metal anode with high areal capacity. *ACS Nano* 2022;16:9105-16. DOI

159. Zhou J, Xie M, Wu F, et al. Encapsulation of Metallic Zn in a Hybrid MXene/Graphene Aerogel as a Stable Zn Anode for Foldable Zn-Ion Batteries. *Adv Mater* 2022;34:e2106897. DOI
160. Wang F, Lu H, Li H, et al. Demonstrating U-shaped zinc deposition with 2D metal-organic framework nanoarrays for dendrite-free zinc batteries. *Energ Storage Mater* 2022;50:641-7. DOI
161. Heo YH, Lee J, Ha S, et al. 3D-structured bifunctional MXene paper electrodes for protection and activation of Al metal anodes. *J Mater Chem A* 2023;11:14380-9. DOI
162. Wei C, Wang Y, Zhang Y, et al. Flexible and stable 3D lithium metal anodes based on self-standing MXene/COF frameworks for high-performance lithium-sulfur batteries. *Nano Res* 2021;14:3576-84. DOI
163. Yang T, Li L, Wu F, Chen R. A soft lithiophilic graphene aerogel for stable lithium metal anode. *Adv Funct Materials* 2020;30:2002013. DOI
164. Hu Z, Su H, Zhou M, et al. Lithiophilic carbon nanofiber/graphene nanosheet composite scaffold prepared by a scalable and controllable biofabrication method for ultrastable dendrite-free lithium-metal anodes. *Small* 2022;18:e2104735. DOI
165. Cao Z, Chen H, Du Z, et al. Low-tortuous MXene (TiNbC) accordion arrays enabled fast ion diffusion and charge transfer in dendrite-free lithium metal anodes. *Adv Energy Mater* 2022;12:2201189. DOI
166. Luo J, Lu X, Matios E, et al. Tunable MXene-derived 1D/2D hybrid nanoarchitectures as a stable matrix for dendrite-free and ultrahigh capacity sodium metal anode. *Nano Lett* 2020;20:7700-8. DOI
167. Xue P, Guo C, Li L, et al. A MOF-derivative decorated hierarchical porous host enabling ultrahigh rates and superior long-term cycling of dendrite-free Zn metal anodes. *Adv Mater* 2022;34:e2110047. DOI
168. Zhang Y, Tian Y, Wang Z, et al. Flexible, free-standing and dendrite-free iron metal anodes enabled by MXene frameworks for aqueous Fe metal dual-ion batteries. *Chemical Engineering Journal* 2023;458:141388. DOI
169. Wu J, Li X, Rao Z, et al. Electrolyte with boron nitride nanosheets as leveling agent towards dendrite-free lithium metal anodes. *Nano Energy* 2020;72:104725. DOI
170. Zhang Y, Huang Z, Wu K, et al. 2D anionic nanosheet additive for stable Zn metal anodes in aqueous electrolyte. *Chem Eng J* 2022;430:133042. DOI
171. Aslam MK, Niu Y, Hussain T, et al. How to avoid dendrite formation in metal batteries: Innovative strategies for dendrite suppression. *Nano Energy* 2021;86:106142. DOI
172. Jiang B, Li F, Hou T, et al. Polymer electrolytes shielded by 2D $Li_{0.46}Mn_{0.77}PS_3$ Li^+-conductors for all-solid-state lithium-metal batteries. *Energ Storage Mater* 2023;56:183-91. DOI
173. Pan Q, Zheng Y, Kota S, et al. 2D MXene-containing polymer electrolytes for all-solid-state lithium metal batteries. *Nanoscale Adv* 2019;1:395-402. DOI PubMed PMC
174. Liu C, Tian Y, An Y, et al. Robust and flexible polymer/MXene-derived two dimensional TiO_2 hybrid gel electrolyte for dendrite-free solid-state zinc-ion batteries. *Chem Eng J* 2022;430:132748. DOI
175. Han X, Chen J, Chen M, et al. Induction of planar Li growth with designed interphases for dendrite-free Li metal anodes. *Energ Storage Mater* 2021;39:250-8. DOI
176. Wu L, Zhang Y, Shang P, Dong Y, Wu Z. Redistributing Zn ion flux by bifunctional graphitic carbon nitride nanosheets for dendrite-free zinc metal anodes. *J Mater Chem A* 2021;9:27408-14. DOI
177. Zhou J, Zhang Z, Jiang W, et al. Ion-sieving Janus separator modified by Ti_3C_2Tx toward dendrite-free zinc-ion battery. *J Alloy Compd* 2023;950:169836. DOI
178. Guo C, Luo ZH, Zhou MX, et al. Clay-originated two-dimensional holey silica separator for dendrite-free lithium Metal Anode. *Small* 2023;19:e2301428. DOI
179. Jiang C, Tang M, Zhu S, et al. Constructing universal ionic sieves via alignment of two-dimensional covalent organic frameworks (COFs). *Angew Chem Int Ed Engl* 2018;57:16072-6. DOI
180. Cao Z, Zhang H, Song B, et al. Angstrom-level ionic sieve 2D-MOF membrane for high power aqueous zinc anode. *Adv Funct Materials* 2023;33:2300339. DOI
181. Ni L, Osenberg M, Liu H, et al. In situ visualizing the interplay between the separator and potassium dendrite growth by synchrotron X-ray tomography. *Nano Energy* 2021;83:105841. DOI
182. Yu SH, Huang X, Brock JD, Abruña HD. Regulating key variables and visualizing lithium dendrite growth: an operando X-ray Study. *J Am Chem Soc* 2019;141:8441-9. DOI PubMed
183. Wu Z, Kong Pang W, Chen L, Johannessen B, Guo Z. In situ synchrotron X-ray absorption spectroscopy studies of anode materials for rechargeable batteries. *Batteries Supercaps* 2021;4:1547-66. DOI
184. Mathew M, Radhakrishnan S, Vaidyanathan A, Chakraborty B, Rout CS. Flexible and wearable electrochemical biosensors based on two-dimensional materials: Recent developments. *Anal Bioanal Chem* 2021;413:727-62. DOI PubMed PMC
185. Xiao X, Zheng Z, Zhong X, et al. Rational design of flexible Zn-based batteries for wearable electronic devices. *ACS Nano* 2023;17:1764-802. DOI
186. Ma Q, Zheng Y, Luo D, et al. 2D materials for all-solid-state lithium batteries. *Adv Mater* 2022;34:e2108079. DOI
187. Wang Q, Lu T, Xiao Y, et al. Leap of Li metal anodes from coin cells to pouch cells: challenges and progress. *Electrochem Energy Rev* 2023:6. DOI
188. Deng S, Jiang M, Rao A, et al. Fast-charging halide-based all-solid-state batteries by manipulation of current collector interface. *Adv Funct Materials* 2022;32:2200767. DOI

189. Duan H, Wang C, Yu R, et al. In situ constructed 3d lithium anodes for long-cycling all-solid-state batteries. *Adv Energy Mater* 2023;13:2300815. DOI